International Journal of Concrete Structures and Materials

RESEARCH

Open Access

Multi-objective Optimisation of One-Part Slag–Flyash–Microsilica Based Alkali-Activated Ternary Binder Mixes

H. M. Jagadisha[1], Poornachandra Pandit[1], Shreelaxmi Prashant[1*], Lalit Bhole[1], Yashodhan Singh[1], Ojas Verma[1] and Mithesh Kumar[1]

Abstract

The study reports the properties of slag–flyash–microsilica ternary blended one-part alkali-activated binder system. Microsilica, characterised by high surface area, helps in reducing porosity and also the presence of active silica contributes enhancing the reactivity of binders, while flyash and GGBS offer aluminosilicates to support alkali activation. Taguchi's design of experiment, integrated with Taguchi grey relational analysis (GRA) is employed to determine the optimal precursor blends, water content and activator dosages to achieve setting times, flow characteristics and compressive strength comparable to conventional OPC. The optimised mix exhibited flowability of 120%, an IST of 46 min, FST of 95 min, and compressive strengths of 54.65 MPa and 69.75 MPa at 7 and 28 days, respectively. The predicted results of the proposed regression model were experimentally validated, with deviations not exceeding 5%. Furthermore, microstructural analyses were performed using a scanning electron microscope (SEM) with energy dispersive X-ray spectroscopy (EDS), X-ray diffraction (XRD), and Fourier transform infrared spectroscopy (FTIR) to examine changes in morphology, mineral phases, and molecular bonding of the binder mixes, respectively. The microanalysis has confirmed formation of dense C/N-A-S-H resembling gels as product of alkali-activation.. Carbon footprint, eco-efficiency and cost analysis were performed and found that the optimised mix is an eco-friendly alternative to OPC-based binders.

Keywords One-part alkali-activation, Multi-objective optimisation, Ternary binder, Microsilica, Taguchi-grey relation analysis, Carbon footprint

*Correspondence:
Shreelaxmi Prashant
shreelaxmi.p@manipal.edu

Graphical Abstract

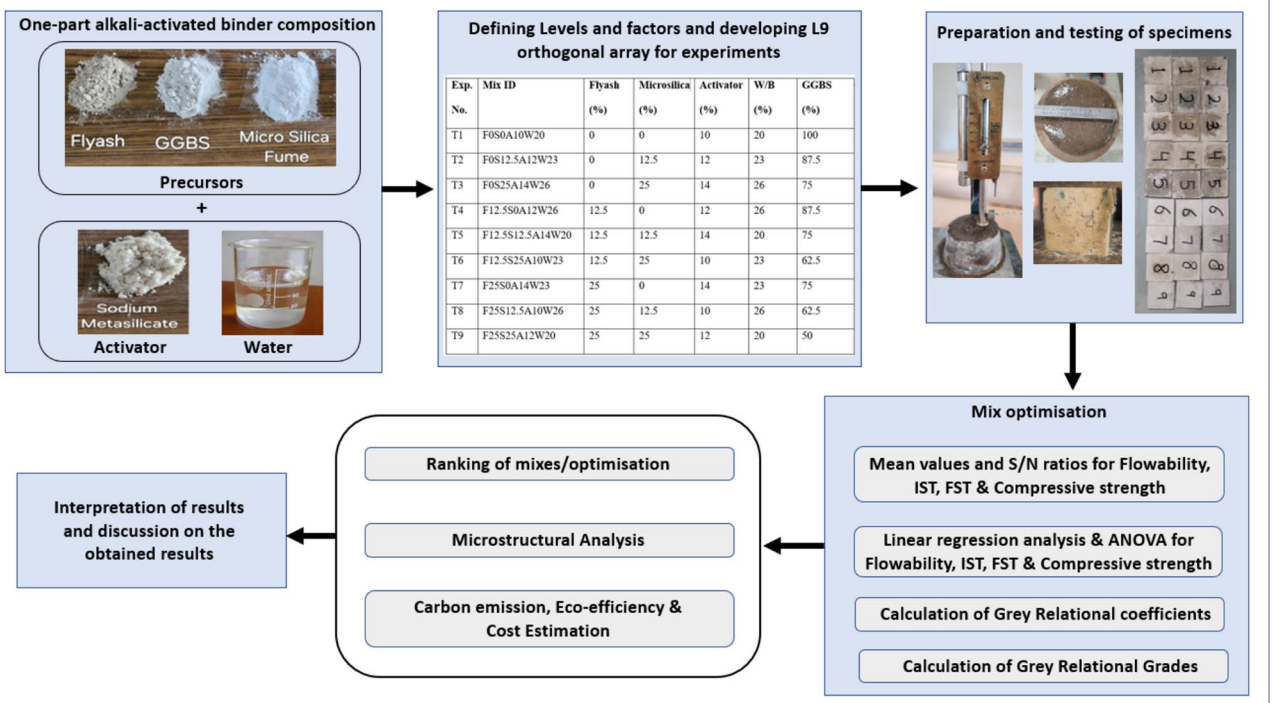

1 Introduction

Ordinary Portland cement (OPC) based binders are widely used in the construction industries because of their mouldability and high compressive strength. As an alternative to OPC-based binder, alkali-activated binders (AAB) are gaining popularity these days because of their eco-friendliness (Fernández-Jiménez et al., 2005; Singh & Middendorf, 2020). AABs system and supplementary cementitious materials gaining popularity because of its low carbon footprint, embodied energy and economical aspects (Alhassan et al., 2023; Faridmehr et al., 2020). The priority on sustainable construction materials aligns with use industrial by-products in large volumes and reduce dependence on natural resources (Alhassan et al., 2023). These binders use industrial and agricultural by-products containing aluminosilicates, used as precursors, that are activated by alkaline activators.

While extensive studies have been conducted on AABs (Ding et al., 2016; Elahi et al., 2020; Farooq et al., 2021; Gok & Sengul, 2024; Kamath et al., 2021), however, its applications to large-scale infrastructure projects are still far from reality. This is because most of the works carried out on alkali-activated materials use the two-part techniques, wherein precursors and liquid activators are mixed to prepare alkali-activated binder systems (Segura et al., 2022; Thatikonda et al., 2024). This is, most often, not suitable for in situ applications and therefore not considered as user-friendly. Combining the user eco-friendliness with the strength and durability requirements is the need of the hour. One-part technology, largely addresses this issue, most efficiently, since it creates a binder phase, combining all the goodness of AABs, yet is user-friendly like the very popular OPC-based binders (Luukkonen et al., 2018; Ma et al., 2018). This consists of aluminosilicate-based precursors that are premixed with solid activators in definite proportions. However, controlling the consistency and setting characteristics is a major challenge, since these properties depend on the composition of the base materials used (Elahi et al., 2020; Luukkonen et al., 2018; Segura et al., 2022; Shah et al., 2020).

Therefore, the properties are not uniform and depend on the source from which they are obtained. This calls for the use of blends of multiple precursors to suit the requirements of fresh and hardened properties. The most commonly used blends, that set at ambient conditions are flyash and GGBS which have proven to be effective binders for structural-grade concrete (Hamsashree et al., 2024; Shah et al., 2020). This combination is becoming increasingly popular among researchers working on alkali-activated materials because both precursors have

the proportions of silica and alumina that support geopolymerisation (Rossi et al., 2022). Only flyash, though activates and forms binder phases like NASH, needs to be supported by heat curing to boost the reaction. On the other hand, GGBS contains higher proportions of calcium oxide, hence sets at ambient temperatures (Hadi et al., 2017; Kamath et al., 2021).

For special applications that demands early strength as well as high ultimate strength, it is apt to use higher proportions of GGBS. Microsilica is yet another promising highly reactive pozzolanic material that has been successfully used in the design of high-strength application to enhance strength and microstructures for specific requirements (Cheah et al., 2017; Deir et al., 2014; Hamada et al., 2023). Typically, microsilica is incorporated at the levels of 10–20% of the total binder content for the development of conventional high-strength concrete with Portland cement as a principal binder. However, in alkali-activated binders, use of higher proportions of microsilica is expected to significantly boost the reactivity of the alkali-activated system, enhancing the polymerisation process (Jaradat & Matalkah, 2023; Mustakim et al., 2021). High silica content in the binder system (combination of flyash and microsilica) promotes the formation of aluminosilicate gels, N-A-S-H or C-S-H in hybrid systems with calcium oxide.

Blends of slag, flyash and microsilica are used as primary precursors in the present study, with varying activator dosages and water content. Slag is associated with early setting and early strength development characteristics, while flyash is associated with enhanced workability and delayed setting times. Incorporation of microsilica, into the one-part binder system, performs a dual role as filler to reduce porosity and enhance the compactness of the binder matrix, due to the presence of finely divided silica, that provides an additional reactive silica source, thereby enhancing the formation of aluminosilicate gels (Perumal et al., 2021; Xi et al., 2022). The proportion of precursors and activator are tailored to achieve required setting times, early strength and long-term stability for precast concrete, 3D printing, and high-performance infrastructure applications (Jaradat & Matalkah, 2023; Mustakim et al., 2021). Since there are many interdependent parameters that simultaneously influence the performance, it is essential to consider the influence of each parameter while proportioning the ingredients of the binder. For enhanced performance, controlling the consistency and setting characteristics is essential. These properties in AABs can be achieved by adjusting the dosages of activators and the water-to-binder ratio. Though activators are essential for initiating the reaction, a higher dosage often leads to quick setting. Hence it is essential to optimise the precursor proportions and activator dosages along with fixing of suitable water-to-binder ratio (Mahendra et al., 2024; Srinivasa et al., 2023). This could necessitate exhaustive experimentation. It is therefore essential to optimise the number of experiments to obtain a suitable mix that combines the properties needed for field applications. Therefore, essential to optimise the number of experiments to obtain a suitable mix that combines the properties needed for field applications (Sheelavantar et al., 2024; Srinivasa et al., 2023).

Design of experiment (DOE) is a statistical tool used for optimisation of processes, to identify the cause-and-effect relations between the input and output variables. The application of Taguchi's DOE approach enables judicious proportioning of constituent ingredients of one-part alkali-activated binder formulations. Taguchi's DOE is a single objective, fractional factorial optimisation technique, used extensively for optimising the number of experiments, while taking into consideration multiple parameters that influence the experimental results. It uses orthogonal arrays to ensure the balance between all the influencing factors and all levels considered. Taguchi GRA offers a systematic approach for multi-objective optimisation, while taking into consideration multiple dependent factors with strength as major factor. This allows to identify the optimal process parameters while considering multiple performance measures simultaneously. This technique possesses the ability to rank parameters based on their influence on the overall performance (Jeffrey Kuo et al., 2011; Mahendra et al., 2024; Panagiotopoulou et al., 2015; Rawat et al., 2022). Table 1 summarises the Taguchi's DOE approach used for the proportioning of precursors and activators in the recent studies. It is evident that researchers have employed varying proportions of binder blends and alkaline activator dosages to achieve suitable fresh and hardened properties. These proportions are mainly aimed at addressing the issues of controlling the setting times and consistency of the binder mix in fresh state as well as achieving required strength and durability in the hardened state. There are multiple factors, most of them interdependent that contribute to the development of the required fresh and hardened properties. This calls for use of a statistical tool that incorporates the effects of multiple influencing parameters and identify the optimal combinations for enhanced performance.

In the current investigation, Taguchi's DOE is selected over other DOEs because of its ability to efficiently screen multiple control factors, with minimal experimental runs, while optimising robustness against noise factors. Additionally, grey relational analysis (GRA) was employed for its systematic approach to normalise multiple conflicting responses into a single performance metric, by avoiding the assignment of relative weights

Table 1 Taguchi's DOE adopted for AAB systems

Type of compositions	DOE employed	Key findings	Reference
Flyash-based geopolymer binder mix	Taguchi method	Optimal conditions to achieve higher compressive strength: Na/Al = 0.85, Si/Na_2O = 1.35 to achieve compressive strength = 43 MPa. The development of strength is primarily governed by the alkali-to-aluminium ratio	(Panagiotopoulou et al., 2015)
One-part alkali-activated self-compacting concrete mixes	Taguchi-grey relational analysis	Slag/FA = 1, Binder content 750 kg/m^3, W/B = 0.45, Na_2O = 5%; to achieve compressive strength = 36.5 MPa The formation of gel products is strongly influenced by the binder proportions and activator dosage	(Mahendra et al., 2024)
Alkali-activated composite binders using waste silica soda lime glass	Taguchi method	Optimal mix is at 0% glass, 60 °C curing temp, 6% Na_2O (28d); 100% glass, 60 °C curing temp, 10% Na_2O (90d) Glass is an effective supplementary material in alkali-activated slag binders	(Martinez-Lopez & Ivan Escalante-Garcia, 2016)
Alkali-activated ladle slag composites binder	Taguchi-based TOPSIS method	Optimum mix composition is 650 kg/m^3 slag, alkali solution/binder = 0.45, Na_2SiO_3/NaOH = 2, crushed sand replacement by dune sand = 25% for strength/workability Their corresponding compressive strength, workability, and IST were 17.9 MPa, 177.5 mm, and 13 min	(Najm et al., 2022)
High-strength AAC	Taguchi method	500 kg/m^3 binder, alkaline activator ratio = 2, activator/binder = 0.5, 12 M NaOH optimal mix developed highest compressive strength = 63.4 MPa	(Kanagaraj et al., 2022)
AAC	Taguchi-grey relational analysis	The optimum mix developed is FA/slag ratio of 90:10, activator liquid/binder ratio of 0.45, 10 M NaOH solution with Na_2SiO_3/NaOH ratio of 1 achieved compressive strength of 40 MPa	(Sheelavantar et al., 2024)
Alkali-activated hybrid binder (slag + OPC)	Taguchi method	The optimum composition of 100% GBFS, 9% Na_2O, solution modulus of 1.0 and W/B ratio of 0.45 achieved the highest 28 days strength of 43.0 MPa	(Amer et al., 2021)
Slag-based geopolymer concrete	Taguchi method and ANOVA	Slag content of 550 kg/m^3, W/B ratio of 0.5 with naphthalene-based admixture achieved the highest 28-day compressive strength 69 MPa	(Amer et al., 2024)

in other multi-objective optimisation techniques. Unlike response surface method, which assumes continuous and well-defined functional relationships, GRA is particularly effective for handling discrete, non-linear, and uncertain data, making it a suitable choice for the present study (Metkar et al., 2013; Shen & Du, 2005).

The construction industry is one of the major contributors to the global warming. Production of cements alone contributes 8% of greenhouse gas emission (Kumar et al., 2022). Sustainability is becoming one of the critical factors, since it uses large volumes of natural resources and the processes involved release huge amounts of carbon into the environment. Reducing the carbon footprint and emphasising on eco-efficiency of a binder system, has main research focus without compromising the mechanical and durability properties.

In the present study, Taguchi and Taguchi GRA were employed for multi-objective optimisation of the one-part slag–flyash–microsilica ternary binder mix to achieve the flowability, setting characteristics and compressive strength suitable for structural applications. Regression equations are proposed to predict compressive strength, setting and flow characteristics that could be achieved with various combinations of the precursors and activators used. The proposed regression equations are then validated with experiments. Microstructural analyses are conducted on mixes to understand the morphology and phases developed.

This paper also aims to evaluate carbon emission, eco-efficiency and cost analysis on optimal binder compositions that balance sustainability, performance, and economic feasibility.

1.1 Research Significance

Present study investigates the properties of a novel slag–flyash–microsilica based one-part alkali-activated binders that are proportioned for optimal level of performances in fresh and hardened states. This research supports the global shift toward low-carbon construction materials, reducing reliance on Portland cement and mitigating CO_2 emissions and enhancing the user friendliness compared to the two-part AAMs. The study aimed at the upcycling of industrial by-products, aligning with circular economy principles and offering sustainable solutions for waste management in industries. The optimised mix demonstrates high compressive strength, making it suitable for precast, 3D printing, and high-performance infrastructure applications.

2 Experimental Investigation

2.1 Materials

Class F flyash, GGBS and microsilica are used as precursors for the present study. The micrographs of these precursors are shown in Fig. 1. Flyash is procured from Bellary Thermal Power Station, Bellary, India. SEM images presented in Fig. 1a reveal that the flyash particles

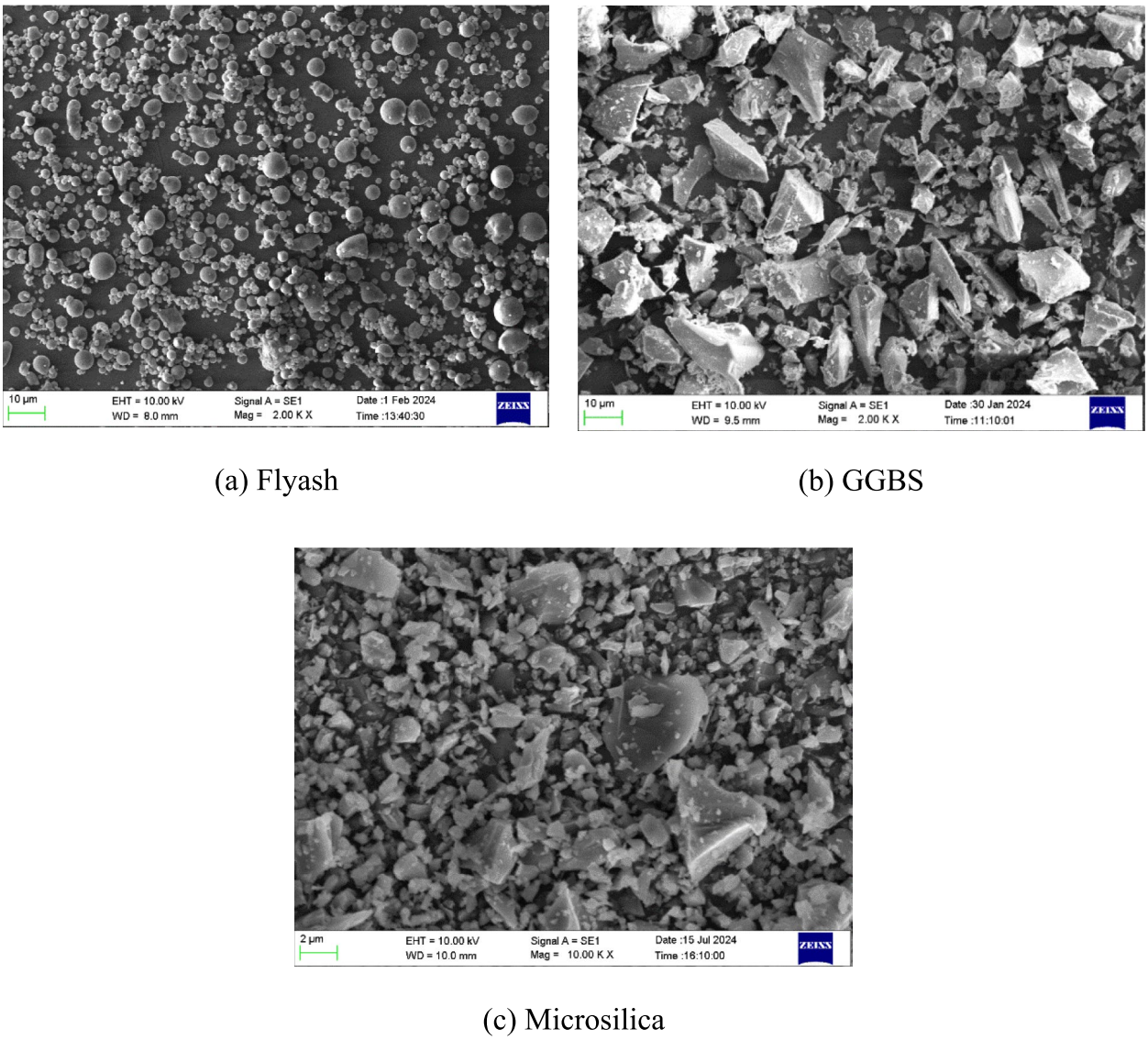

Fig. 1 SEM micrographs of **a** flyash, **b** GGBS, **c** microsilica

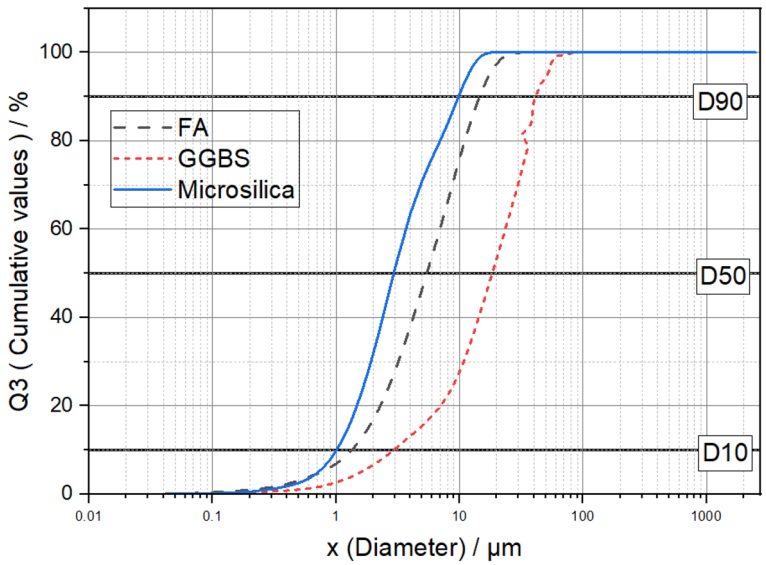

Fig. 2 Particle size distribution of precursors

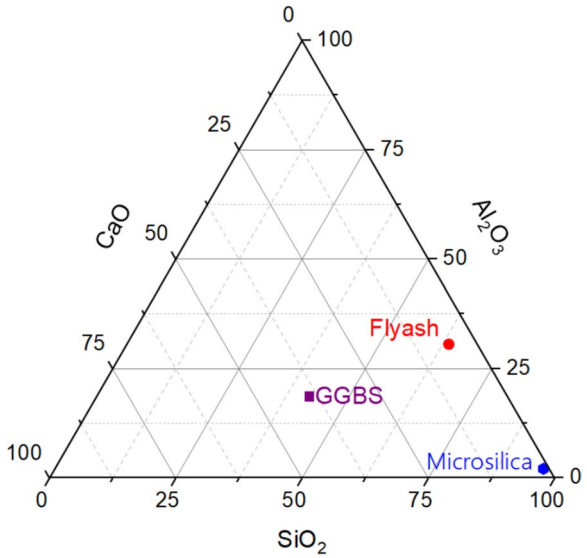

Fig. 3 Ternary plot of precursors

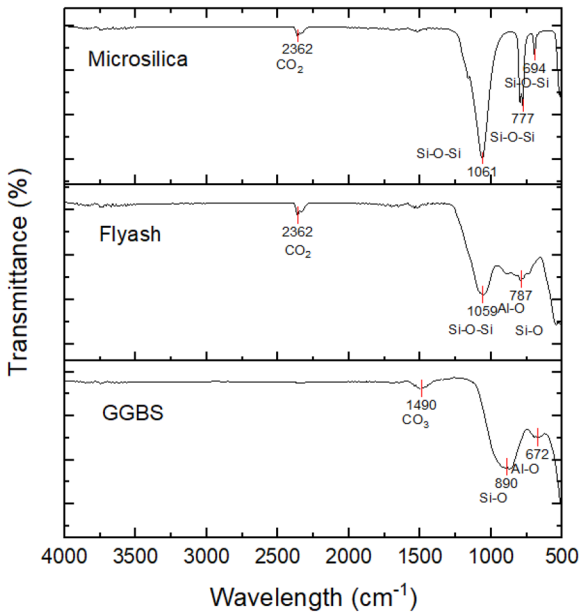

Fig. 4 FTIR spectra of microsilica, flyash and GGBS

are spherical, with sizes ranging from 0.04 µm to 32 µm, as determined by particle size distribution (PSD) analysis shown in Fig. 2. Flyash, with specific gravity of 2.3, is primarily composed of silica and alumina as confirmed by oxide compositions presented in Fig. 3. These compositions are further validated by the characteristic peaks observed in the FTIR spectrum shown in Fig. 4. The primary absorption bands of silica, indicating the Si–O–Si stretching bond, are observed as a broad band around 1059 cm^{-1}. The presence of the Al–O–Al stretching bond is confirmed by peaks identified around 787 cm^{-1}, indicating the Al–O–Al bond (Mahendra et al., 2024). Figure 5 represents the XRD spectra of flyash. The occurrence of amorphous phases accompanied by minerals like quartz, mullite, calcite, and hematite are identified (Puligilla & Mondal, 2013; Srinivasa et al., 2023; Yousefi Oderji et al., 2019).

GGBS is procured from JSW Steel, Bellary, India. GGBS, as appears in micrograph Fig. 1b, consists of irregular and angular-shaped particles with a size ranging

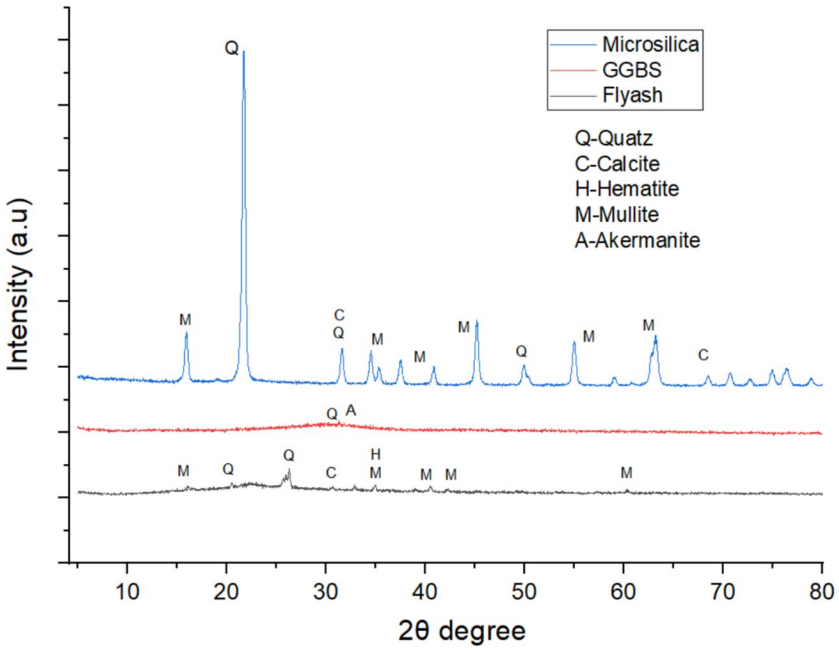

Fig. 5 XRD spectra of precursors

from 0.04 µm to 112 µm as per PSD data presented in Fig. 2. GGBS with a specific gravity of 2.3, is primarily composed of calcium silicates and aluminosilicates as shown in Fig. 3. FTIR spectrum of GGBS shown in Fig. 4 represents a strong broad band identified around 890 cm^{-1}, indicating Si–O stretching vibrations. Al–O stretching bands are identified around the 672 cm^{-1}. Weak carbonate peak is also identified around 1490 cm^{-1}. Figure 5 represents XRD spectra for GGBS, indicating the presence of an amorphous mineral phase, with small two peaks that can be associated with calcite and akermanite (Mahendra et al., 2024; Puligilla & Mondal, 2013).

Microsilica, procured from Astra Chemicals, Chennai, India, is used in the present study as one of the precursors. Figure 1c presents the micrograph of microsilica, wherein fine particles with irregular shapes and sharp edges are visible. The particle sizes range from 0.04 µm to 18 µm as per the PSD analysis shown in Fig. 2. Microsilica with specific gravity 2, predominantly comprises amorphous form of SiO_2 as represented in Fig. 3, that can be suitably used as a pozzolanic material in concrete (Hamada et al., 2023). Peaks identified in FTIR at 1061 cm^{-1}, 777 cm^{-1} and 694 cm^{-1} indicate the presence of asymmetrical and symmetric stretching vibrations of Si–O–Si linkages, respectively (Szabó & Mucsi, 2020). Figure 5 represents the XRD spectrum of the microsilica with the peaks of quartz, mullite and calcite. Sodium metasilicate powder procured through Astra Chemical, Chennai, India, is used as a solid activator in the present research work. Sodium metasilicate (Na_2SiO_3) is a white inorganic salt characterised by its high alkalinity and water solubility and a density of 2.4 g/cm^3. The ratio of total alkalinity (expressed as Na_2O) to total soluble silica (as SiO_2) is approximately 1:1, with a tolerance of ±0.05. The oxide compositions and physical parameters of precursors are listed in Table 2.

Table 2 Parameters of precursors

Parameters	Flyash	GGBS	Microsilica
Chemical properties (oxides compositions in percentage %)			
SiO_2	53.25	37.30	94.3
Al_2O_3	25.62	16.60	2.1
Fe_2O_3	6.4	0.37	0.78
CaO	4.7	34.70	0.55
TiO_2	1.92	0.82	-
MgO	1.04	6.87	0.5
MnO	0.07	0.96	-
Na_2O	2.22	0.31	-
K_2O	2.05	0.63	-
SO_3	1.29	1.35	0.58
Loss of ignition	1.4	–	1.18
Physical parameters			
Specific gravity	2.3	2.28	2
Average particle size (µm)	6.87	22.31	4.23

2.2 Optimisation of Binder Composition

2.2.1 Taguchi Method

In the present study, Taguchi's DOE is adopted with 4 factors and 3 levels of variation. The 4 factors considered are percentage of flyash, percentage of microsilica, water content expressed as a percentage of total binder and percentage of activator. These factors are varied at 3 levels to optimise the binder compositions as shown in Table 3. The optimisation is carried out using Minitab software. Table 4 shows the set of experiments, designed based on Taguchi's L9 orthogonal array for the current investigation. The mixes are designated as per their precursor compositions. The mix ID F0S0A10W20 represents F0- 0% flyash, S0- 0% microsilica, A10- 10% activator and W20- 20% water content expressed as weight of water to binders (W/B). This means that the precursor contains 100% GGBS.

The Taguchi loss function is generally transformed into a signal-to-noise (S/N) ratio, where "signal" represents the desirable effects and "noise" represents the undesirable effects of the output characteristics. In S/N ratio analysis, the quality characteristics are typically classified into three categories: lower-the-better, nominal-the-better, and higher-the-better (Hadi et al., 2017; Jeffrey Kuo et al., 2011; Karthik & Mohan, 2021). In the present investigation, GGBS is used as main precursor which possesses quick setting characteristic. It is essential to delay the setting to make it suitable for field applications.

Table 3 Levels and factors used in the Taguchi method

Factors	Level 1	Level 2	Level 3
Flyash	0%	12.5%	25%
Microsilica	0%	12.5%	25%
W/B	24%	27%	30%
Activator	10%	12%	14%

The maximum value of FST is not allowed to exceed 600 min as per the specifications stipulated in IS 12269–2013 (*IS 12269: Ordinary Portland Cement, 53 Grade—Specification*, 2013). Hence, higher-the-better approach is adopted, by aiming for standard flowability, strength and setting time within L9 orthogonal mixes (Mahendra et al., 2024; Sheelavantar et al., 2024).

Further, main effect analysis is performed by creating a response graph and conducting the analysis of variance (ANOVA) for determining the S/N ratio to understand the level of significance of every parameter in refining the binder performance (Mustapha et al., 2021). From the Taguchi method, the significant factors that influence the properties such as flowability, setting time and strength are obtained independently. However, to examine the combined effect of these parameters, the combination of GRA with the Taguchi method is employed for multi-objective optimisation (Hadi et al., 2017; Jeffrey Kuo et al., 2011; Karthik & Mohan, 2021).

2.2.2 Taguchi Grey Relation Analysis (GRA)

The Taguchi-DOE approach is an effective statistical tool for maximising a single response variable, whereas Taguchi-GRA is opted when the experimentation deals with multiple interdependent variables. Optimisation procedure adopted in the present study consists of normalising the calculated S–N ratios in the range of 0 to 1. Followed by computing the deviational sequences and determining the grey relational coefficients to represent the interaction effects between the expected results and the actual data. Further, grades are ranked according to the average grey relational coefficients and their significance (Mahendra et al., 2024; Rawat et al., 2022; Sheelavantar et al., 2024).

2.3 Specimen Preparation and Testing Methods

The precursors, namely GGBS, flyash, and microsilica in the proportions mentioned in Table 2 along with

Table 4 L9 orthogonal array based on Taguchi method

Exp. no.	Mix ID	Flyash (%)	Microsilica (%)	Activator (%)	W/B (%)	GGBS (%)
T1	F0S0A10W20	0	0	10	20	100
T2	F0S12.5A12W23	0	12.5	12	23	87.5
T3	F0S25A14W26	0	25	14	26	75
T4	F12.5S0A12W26	12.5	0	12	26	87.5
T5	F12.5S12.5A14W20	12.5	12.5	14	20	75
T6	F12.5S25A10W23	12.5	25	10	23	62.5
T7	F25S0A14W23	25	0	14	23	75
T8	F25S12.5A10W26	25	12.5	10	26	62.5
T9	F25S25A12W20	25	25	12	20	50

sodium metasilicate powder as an activator were used to develop binder mixes. Specified proportions of each of these ingredients are weighed and initially dry mixed for 2–3 min in the Hobart mixer. Dry mixing of all precursors and activator is continued until the mass appears uniform and homogeneous. Later the predetermined amount of water to the dry blends is added in the Hobart mixer. The ingredients added were thoroughly mixed for about 3–4 min at a speed of 65 rpm until a consistent and homogeneous paste was obtained. The prepared binder mixes were later tested for their flowability test as per IS 5512 (IS 5512: Specification for Flow Table for Use in Tests of Hydraulic Cements and Pozzolanic Materials, 1983) and setting time as per 4031 (5) (*IS 4031–5: Methods of Physical Tests for Hydraulic Cement, Part 5: Determination of Initial and Final Setting Times*, 2005). The paste is then poured into 50 mm cube moulds. For each mix, six cubes were cast, and 3 were tested at 7 days and the remaining 3 cubes are tested at 28 days, curing period. The cast specimens were cured under ambient conditions until testing. The average compressive strength of ambient cured specimens are tested at 7 days and 28 days of curing period, as per specifications stipulated in IS 4031 (6) (*IS 4031-6: Methods of Physical Tests for Hydraulic Cement Part 6: Determination of Compressive Strength of Hydraulic Cement Other than Masonry Cement*, 2005).

2.4 Microstructural Analysis

Microanalysis of the binder pastes using SEM–EDS, FTIR and XRD techniques were performed on all binder specimens to determine the morphologies and identify the crystalline phases and functional groups to characterise the alkali-activation products. All the samples used for these tests were extracted from small fragments of binders, collected after the cube specimens were subjected to compressive loads until failure, to determine the 28 days of compressive strength. SEM images were obtained using ZEISS EVO MA18 with Oxford EDS, having a minimum of 1× and a maximum of 1,00,000× of magnification range. Gold-sputtering was used to obtain information about the morphology and elemental compositions of the binder specimen. FTIR analysis was performed using Bruker Alpha II spectrometer equipped with attenuated total reflectance mode. The spectrometer operates within spectral range of 6000 cm^{-1} to 500 cm^{-1} with spectra resolution 4 cm^{-1}. XRD technique is performed to identify the phases developed of the binder specimen after 28 days of curing. Rigaku Miniflex 600, 5th generation, X-ray generation upto 40 kV & current (15 mA) instrument is used. The X'Pert high scores software was used to carry out the phase analysis to identify the binder phases developed.

2.5 Sustainability Assessment: Carbon Emissions and Cost Analysis

The environmental impact and economic aspects of the proposed AAB systems are assessed through carbon footprint, eco-efficiency and cost analysis. The obtained results are compared with those of conventional OPC binders using a cradle-to-gate life cycle assessment approach. While the optimisation of mixes is primarily aimed to attain desirable strength and fresh-state characteristics, the sustainability evaluation serves to confirm their environmental viability.

3 Results and Discussion

3.1 Responses from Taguchi Method

3.1.1 Flowability

Flowability test was conducted on all L9 orthogonal mixes (T1 to T9), considering the four parameters that influence the flowability. These are flyash content, water content (W/B), microsilica content, and the activator dosage. From Fig. 6, the mix T1 (F0S0A10W20) is observed to have the lowest flow value of 10%, whereas the mix T4, T7 and T8 (F12.5S0A12W26, F25S0A14W23 and F25S12.5A10W26) are characterised with the highest flow value of 150%. The flowability of mixes gets enhanced with the increase in the water content (W/B) and the activator dosage. The mean S–N ratio plots of the flowability of mixes listed are illustrated in Fig. 7a. The water content (W/B), which is Ranked 1, was identified as the most influential parameter for achieving enhanced flow values, followed by flyash content (Rank 2) and the activator dosage (Rank 3). With the inclusion of microsilica from level 1 to level 2, there is an increase in flowability observed. Further increase in microsilica content, to level 3, i.e. 25%, resulted into a drastic decrease in flowability. This is because the microsilica is characterised by high surface area, which has correspondingly resulted into higher water demand (Thatikonda et al., 2024). The optimal combination of these parameter levels yielded to the most favourable response, ensuring the flowability levels of 110% ± 5% as per ASTM C1437–01(*ASTM C1437-01: Standard Test Method for Flow of Hydraulic Cement Mortar*, 2020). The results reveal that the optimal parameters for maximising the flowability characteristics are microsilica at 12.5%, W/B at 26%, and activator at 14% as shown in Fig. 7a.

3.1.2 Setting Times

The L9 mix proportions were tested for their IST and FST using the standard Vicat apparatus. Figure 8 illustrates the results of IST and FST. The IST of the mixes varied between 35 to 60 min, depending on the proportions used in precursor blends. Similarly, the FST varied from 65 to 124 min. Amongst the mixes studied,

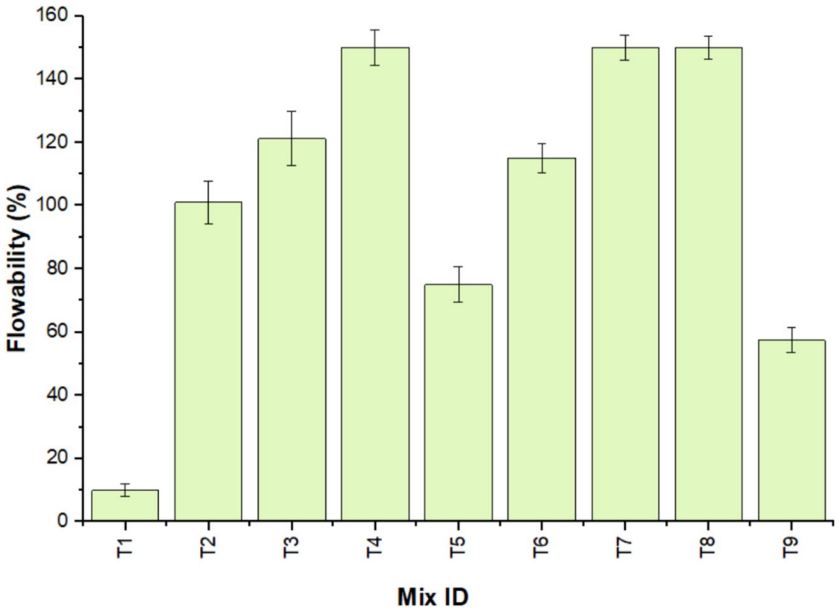

Fig. 6 Flowability response of L9 orthogonal array

T5 (F12.5S12.5A14W20) exhibited the quickest setting characteristics, while T4 (F12.5S0A12W26) and T8 (F25S12.5A10W26) mixes have exhibited the highest IST and FST, respectively.

The mean S–N ratio plots of the IST and FST listed are illustrated in Fig. 7b and c, respectively. For initial setting, the activator dosage is ranked 1 which means the activator dosage highest influence on setting. Higher activator content in the binders corresponds to early dissolution of the precursors leading to faster setting. This is followed by the W/B, which is Ranked 2. The microsilica content in the binder is ranked 3, and the flyash content ranked 4. Microsilica is characterised with smaller particle size, hence will react faster compared to flyash and thereby contribute more to early setting than flyash.

Figure 7b shows that the initial setting time increases with the increase in W/B, due to the significant influence of water content in delaying the reaction process (Kamath et al., 2021; Sheelavantar et al., 2024). However, increase in activator, shows a significant drop in setting time. From Taguchi's analysis, the optimum levels obtained for the IST are microsilica at 0%, W/B at 26%, flyash at 12.5%, and activator dosage at 12%.

Similarly, for FST the significant factors, as obtained by Taguchi's S–N analysis are activator dosage (Rank 1), followed by water content (W/B) (Rank 2), flyash content (Rank 3) to obtain longer FST. The optimal parameter levels for FST are identified as 0% microsilica, 26% W/B, 25% flyash, and 10% activator.

3.1.3 Compressive Strength

Figure 9 shows the 7 days and 28 days compressive strength response of one-part alkali-activated binder specimens, for all mixes used in the present study. From the results, it is evident that the mix T1 (F0S0A10W20), characterised with 0% flyash, 20% water content (W/B), 10% activator content, and 0% microsilica, developed the lowest compressive strengths of 31.18 MPa and 32 MPa, respectively, after 7 and 28 days of ambient curing. On the other hand, the mixes T3 (F0S25A14W26), T6 (F12.5S25A10W23) and T9 (F25S25A12W20) achieved relatively higher 7 days compressive strength compared to other L9 mixes. These compositions contain 25% microsilica, higher than generally used in OPC-based binder compositions, resulting into higher strength development. The presence microsilica in higher proportions provides large surface areas, which resulted into enhanced dissolution of oxides thereby resulting into early strength development and pore-filling. (Luukkonen et al., 2018; Rostami & Behfarnia, 2017; Wang et al., 2022). The mixes T5 (F12.5S12.5A14W20) and T7 (F25S0A14W23) exhibit the highest compressive strengths after 28 days of ambient curing, where activator and microsilica content plays vital role in the 28 days strength development.

The mean S–N ratio plots for 7 days and 28 days compressive strengths of all the mixes are illustrated in Fig. 7d and e. Increments in the levels of microsilica content and activator dosage results into greater mean S–N ratios for 7 days compressive strength as evident in Fig. 7d.

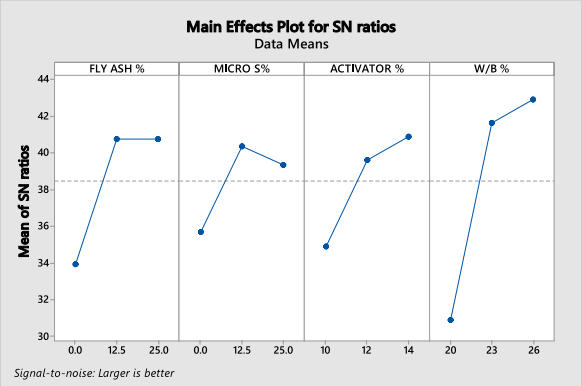

(a) S-N ratios of Flowability test

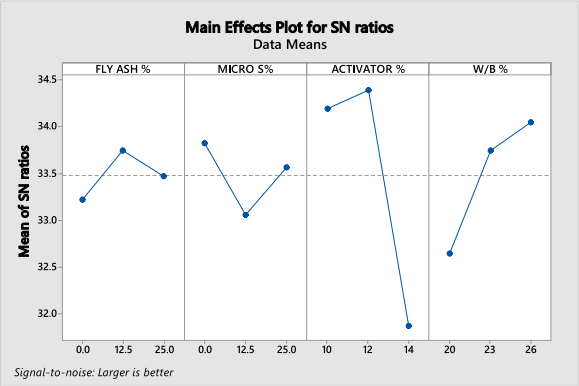

(b) S-N ratios of IST

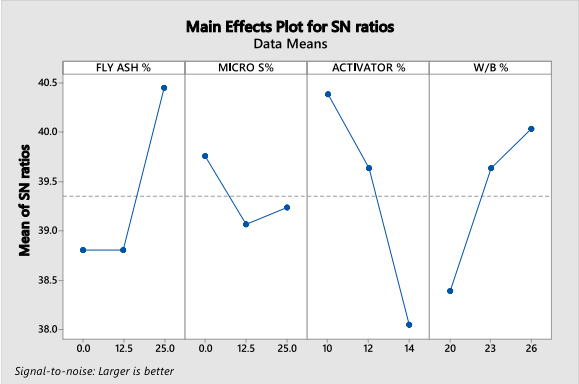

(c) S-N ratios of FST

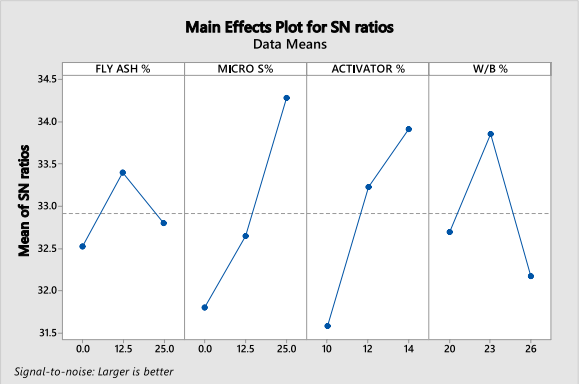

(d) S-N ratios of 7 days compressive strength

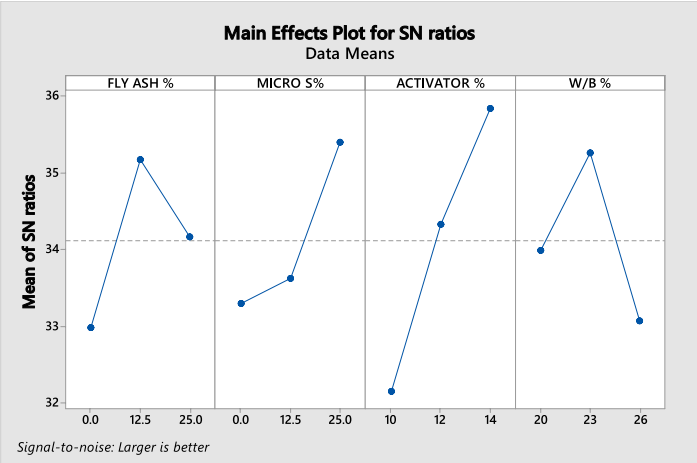

(e) S-N ratios of 28 days compressive strength

Fig. 7 Main effects plot for S–N ratios of **a** flowability test, **b** IST, **c** FST, **d** 7 days compressive test, and **e** 28 days compressive test

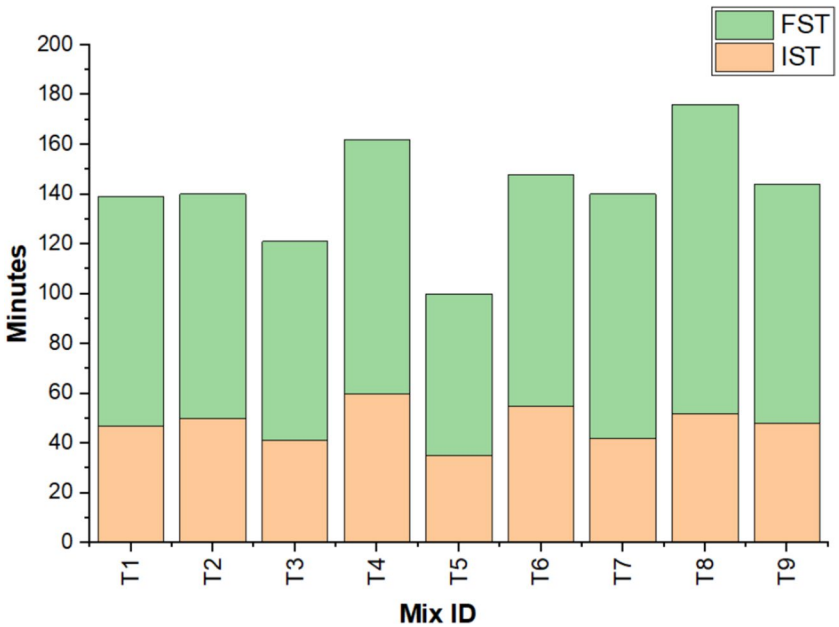

Fig. 8 Initial setting and final setting time responses of L9 orthogonal array mixes

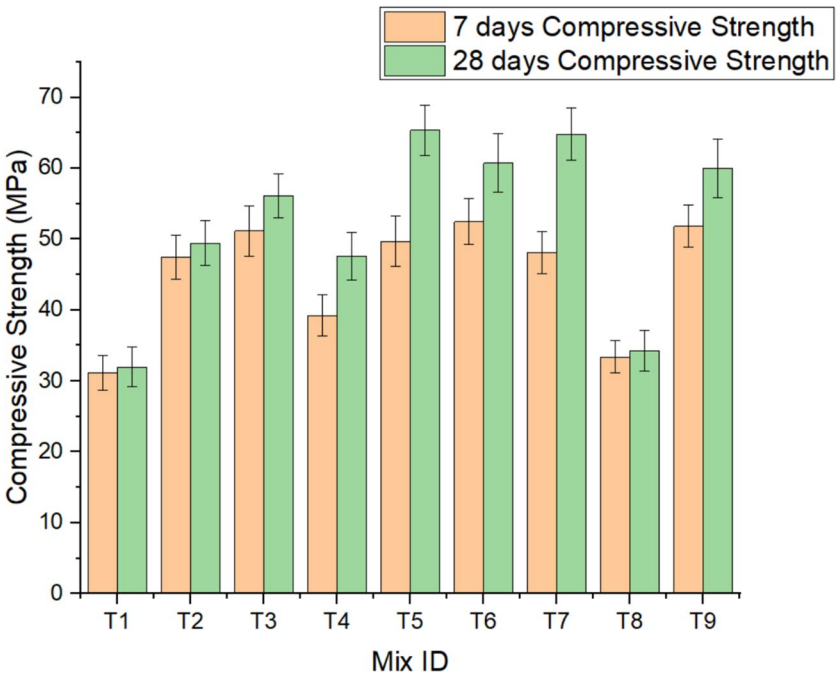

Fig. 9 Compressive strength response of L9 orthogonal array

As the levels of W/B increases, the mean S–N value dropped significantly. This is because the performance of the alkali-activated binder mix is negatively influenced by the increase in the water content (W/B) because the concentration of activators gets diluted with increase in water content in the binder system, thereby resulting into development of lower compressive strength (Geraldo et al., 2023; Yusslee & Beskhyroun, 2023). Therefore, for 7 days compressive strength, microsilica content (Rank 1) is the most significant parameter, followed by the activator dosage (Rank 2), water content (W/B) (Rank 3) as per S–N curves. From S–N analysis, it is found that, the

optimum levels for 7 days compressive strength are flyash at 12.5%, water content (W/B) at 23%, activator at 14%, and microsilica at 25%. A similar pattern is observed in the mean S–N ratios of the 28-day compressive strength, as depicted in Fig. 7e.

Increments in levels of activator dosage and microsilica content results in greater mean S–N ratios for 28 days compressive strength. However, the compressive strength mean S–N ratio falls with the increase in W/B ratio beyond 23%. From S–N analysis, it is found that, the optimum levels required for obtaining highest 28 days compressive strength is flyash at 12.5%, water content (W/B) at 23%, activator at 14%, and microsilica at 25%. It is noticed that activator dosage (Rank 1) is the most influencing parameter, followed by microsilica content (Rank 2), water content (W/B) (Rank 3) that influence the 28 days compressive strength development characteristics of the binder.

Linear regression equations were developed to predict individual responses, including dependent variables like compressive strength after 28 days, flowability, and IST and FST. The dependent variables are expressed as linear functions of flyash%, water content (W/B) %, activator (%), and microsilica%. The linear regression equations are as follows:

$$\begin{aligned}\text{Flowability (\%)} &= -342.3 + 1.670\ \text{Flyash \%} \\ &\quad - 0.217\ \text{Microsilica \%} \\ &\quad + 5.94\ \text{Activator \%} + 15.49\text{W}/\text{B \%}\end{aligned}$$

$$\begin{aligned}\text{Initial setting time (min)} &= 54.6 + 0.053\ \text{Flyash \%} \\ &\quad - 0.067\ \text{Microsilica \%} \\ &\quad - 3.00\ \text{Activator \%} + 1.278\text{W}/\text{B \%}\end{aligned}$$

$$\begin{aligned}\text{Final setting time (min)} &= 92.7 + 0.747\ \text{Flyash \%} \\ &\quad - 0.213\ \text{Microsilica \%} \\ &\quad - 6.08\ \text{Activator \%} + 2.944\text{W}/\text{B \%}\end{aligned}$$

$$\begin{aligned}\text{Comp strength 7 days (MPa)} &= 17.8 + 0.047\ \text{Flyash \%} \\ &\quad + 0.492\ \text{Microsilica \%} \\ &\quad + 2.66\ \text{Activator \%} - 0.496\text{W}/\text{B \%}\end{aligned}$$

$$\begin{aligned}\text{Comp strength 28 days (MPa)} &= 8.8 + 0.287\ \text{Flyash \%} \\ &\quad + 0.433\ \text{Microsilica \%} \\ &\quad + 4.94\ \text{Activator \%} - 1.08\text{W}/\text{B\%}.\end{aligned}$$

3.1.4 Analysis of Variance (ANOVA) Results for Responses of Taguchi Method

In combination with the Taguchi method, the analysis of variance (ANOVA) is yet another statistical tool employed to quantify the percentage contribution of each parameter. ANOVA aids in identifying the importance of various factors influencing the optimisation of a variable's performance (Mustapha et al., 2021). Table 5 outlines the ANOVA results for SN ratios for dependent variables.

Table 5 Analysis of variance for SN ratios for flowability, IST, FST and compressive strength

Source	DF	Seq SS	Adj SS	Adj MS	% Contribution
Analysis of variance for SN ratios of flowability					
FLY ASH %	2	93.179	93.179	46.589	20.71%
MICROSILICA%	2	36.538	36.538	18.269	8.123%
ACTIVATOR %	2	59.513	59.513	29.756	13.231%
W/B %	2	260.555	260.555	130.277	57.928%
Total	8	449.784			
Analysis of variance for SN ratios of IST					
FLY ASH %	2	0.4139	0.4139	0.20694	2.53%
MICROSILICA%	2	0.9025	0.9025	0.45127	5.52%
ACTIVATOR %	2	11.7925	11.7925	5.89627	72.08%
W/B %	2	3.2513	3.2513	1.62564	19.87%
Total	8	16.3602			
Analysis of variance for SN ratios of FST					
FLY ASH %	2	5.3618	5.36182	2.68091	28.15%
MICROSILICA%	2	0.7713	0.77130	0.38565	4.05%
ACTIVATOR %	2	8.5174	8.51736	4.25868	44.71%
W/B %	2	4.3966	4.39657	2.19828	23.083%
Total	8	19.0470			
Analysis of variance for SN ratios of 7 days compressive strength					
FLY ASH %	2	1.1930	1.19298	0.59649	4.99%
MICROSILICA%	2	9.6110	9.61104	4.80552	40.27%
ACTIVATOR %	2	8.6068	8.60681	4.30341	36.06%
W/B %	2	4.4555	4.45547	2.22773	18.68%
Total	8	23.8663			
Analysis of variance for SN ratios of 28 days compressive strength					
FLY ASH %	2	7.1836	7.1836	3.5918	16.83%
MICROSILICA%	2	7.7141	7.7141	3.8571	18.077%
ACTIVATOR %	2	20.5555	20.5555	10.2777	48.17%
W/B %	2	7.2186	7.2186	3.6093	16.91%
Total	8	42.6717			

As per the ANOVA results for flowability, water content (W/B) is the most influencing parameter, as it accounts to 57.92% contribution, followed by flyash and activator dosage with a contribution of 20.71% and 13.23%, respectively. Microsilica content is the least influencing parameter having a contribution of only 8.12%.

The IST is influenced by the activator dosage, since the initiation of activation depends on how well the precursors dissolute into the alkaline media, which in turn depends on the dosage of activators. The activator is therefore rated as the most influential parameter contributing to about 72.08%. This is followed by water content W/B and microsilica with a contribution

of 19.87% and 5.52%, respectively. Flyash content is the least influencing parameter with a contribution of only 2.53%. Activator dosages need to be fine-tuned in order to achieve the setting characteristics to suit the project requirements. The FST is also influenced most by the activator dosage with a contribution of about 44.71%, followed by flyash and water content (W/B) with a contribution of 28.15% and 23.08%, respectively. Microsilica is the least influencing parameter having a contribution of only 4.05%.

Microsilica is the most influential parameter, contributing 40.27% to the development of 7-day compressive strength. This is attributed to the high reactivity and pore-filling properties of microsilica, which enhances early-age strength by promoting denser microstructure formation. The activator concentration was the second most influential factor, contributing 36.06% to the compressive strength. Activator plays a critical role of alkali activation in AAB systems, where higher alkalinity typically accelerates geopolymerisation, leading to improved early strength. The W/B ratio exhibited a moderate influence (18.68%), followed by flyash as the least influencing parameter having a contribution of only 4.99%. The activator concentration emerged as the most dominant factor, contributing 48.17% to the 28-day compressive strength. The contribution of microsilica content and W/B of 18.07% and 16.91%, respectively, is noted as per ANOVA. Flyash is ranked as the least influencing parameter having a contribution of about 16.83%.

3.2 Multi-objective Optimisation Using Grey Relation Analysis

The computed values of the variables used in the Taguchi-GRA phases for the one-part alkali-activated binder mixes examined are shown in Table 6. The mix T6, with grey relational grade (Γ) of 0.895 is designated as best amongst the L9 orthogonal mixes presented in this work.

The mean grey relational grade (Γ) for each parameter was computed in order to get the overall best one-part alkali-activated binder mix. Amongst all the values of the parameter considered, the one with the largest mean Γ value is considered as the best, since it will have the highest influence on the responses.

3.2.1 Response Relation Grade

The optimised proportions of precursors and activator is obtained by using response relation grade, which takes into consideration the influence of each factor at all the defined levels (Mahendra et al., 2024; Sheelavantar et al., 2024). The grey relational grade, for each of the parameters considered and their levels, is tabulated in Table 7. The highest mean grey-relational grade corresponding

Table 6 Calculated values of Taguchi-GRA analysis

Mix ID	S–N ratios for responses					Normalisation of SN ratios					Grey relation coefficients of SN ratios					Grade (Γ)	Rank
	FL %	IST	FST	CS* 7D	CS* 28D	FL %	IST	FST	CS* 7D	CS* 28D	FL %	IST	FST	CS* 7D	CS* 28D		
T1	20.0	33.44	39.28	29.88	30.1	0.0	0.55	0.54	0.00	0.00	0.33	0.52	0.52	0.33	0.33	0.44	9
T2	40.09	33.98	39.08	33.53	33.88	0.85	0.66	0.50	0.81	0.61	0.77	0.60	0.50	0.72	0.56	0.695	8
T3	41.67	32.26	38.06	34.17	34.98	0.92	0.29	0.32	0.95	0.79	0.86	0.41	0.42	0.91	0.70	0.743	5
T4	43.52	35.56	40.17	31.87	33.55	1.00	1.00	0.70	0.44	0.56	1.00	1.00	0.62	0.47	0.53	0.775	4
T5	37.50	30.88	36.26	33.93	36.31	0.74	0.00	0.00	0.90	1.00	0.66	0.33	0.33	0.83	1.00	0.722	6
T6	41.21	34.81	40.00	34.40	35.67	0.90	0.84	0.67	1.00	0.90	0.84	0.76	0.60	1.00	0.83	0.895	1
T7	43.52	32.46	39.82	33.64	36.23	1.00	0.34	0.64	0.83	0.99	1.00	0.43	0.58	0.75	0.98	0.833	2
T8	43.52	34.32	41.87	30.48	30.70	1.00	0.73	1.00	0.13	0.10	1.00	0.65	1.00	0.37	0.36	0.711	7
T9	35.19	33.62	39.65	34.29	35.56	0.65	0.59	0.60	0.98	0.88	0.59	0.55	0.56	0.95	0.81	0.778	3

* CS 7D and 28D: compressive strength of 7 days and 28 days, FL-Flowability

Table 7 Response for mean grey relation grade

Factors	Level 1	Level 2	Level3	Max	Min	Delta	Rank
Response relation grade							
Flyash	0.63	0.80	0.77	0.80	0.63	0.17	1
Microsilica	0.68	0.71	0.81	0.81	0.68	0.12	3
Activator	0.68	0.75	0.77	0.77	0.68	0.08	4
W/B	0.65	0.81	0.74	0.81	0.65	0.16	2

to the flyash content is 12.5% which is level 2. The next influencing parameter is the water content, corresponding to the grey-relational grade of 23% at level 2, while that of activator dosage is 14% at level 3, and microsilica content of the binder mix stands at 25% at level 3. Table 8 lists the optimum parameter values for individual responses based on the Taguchi method and the Taguchi GRA method. The optimised mix exhibited flowability of 120%, an IST of 46 min, FST of 95 min, and compressive strengths of 54.65 MPa and 69.75 MPa at 7 and 28 days, respectively. Calcium oxide-rich GGBS is a precursor with high reactivity, that accelerate geopolymerisation at ambient cured conditions (Provis & Bernal, 2014). In contrast, microsilica promotes accelerated dissolution leading to enhanced pore-filling effect thereby reducing porosity (Luukkonen et al., 2018; Rostami & Behfarnia, 2017; Wang et al., 2022). This is evident from SEM micrographs of the L9 orthogonal mixes.

For validation, binder mixes were casted into cubes of proportions not listed in L9 orthogonal array and tested for setting times, flowability and compressive strengths. The proportions of mixes that are selected for validation are listed in Table 9. The test results obtained are compared with the values predicted using linear regression equations derived from Taguchi analysis. The observed variation between the experimental and predicted results lie within a range of ± 6%, as detailed in Table 9. This demonstrates a strong correlation between the predicted values and the actual experimental results, highlighting the reliability and precision of the predictive models and confirming their effectiveness for practical applications.

3.3 Microstructural Analysis

Microstructural analysis of the binder samples helps in understanding the behaviour, reactivity, morphology at microlevels that influence the mechanical properties of the mixes. The SEM–EDS, FTIR and XRD results provided insights into the microanalysis of the binder matrix. These microstructural analyses are performed on the fractured binder specimens collected after 28 days of the compressive strength test.

Table 9 Validation for proposed Taguchi's regression equations

Sample	Responses	Actual	Predicted	Error %
F10 S10 A11 W25	Flowability	122.5	124.273	− 1.45
	IST	55	53.41	2.90
	FST	110	104.76	4.76
	CS 7 days*	42.46	40.05	5.67
F20 S20 A13 W22	Flowability	110	103.66	5.76
	IST	45	43.436	3.47
	FST	92	89.108	3.14
	CS 7 days*	51.31	52.248	− 1.83
F15 S15 A14 W24	Flowability	132.5	133.5945	− 0.83
	IST	45	43.062	4.31
	FST	90	86.246	4.17
	CS 7 days*	52.62	51.221	2.66

* CS 7 days: compressive strength of binder at 7 days age

3.3.1 SEM and EDS Analysis

The SEM images of L9 orthogonal mixes are presented in Fig. 10. The micrographs reveal the continuous gelatinous formations throughout the microstructures of all the mixes. These dense and cohesive structural formations are primarily composed of the C/N-A-S-H gels, contributing to the binder strength. The mixes T5, T7 and T6 exhibit continuous gelatinous formations, indicating the occurrence of higher degree of polymerisation between the activator and precursors, contributing to the high compressive strength. In these mixes, activators and precursors are completely polymerised and form a dense matrix, which is also reflected in the compressive strength of these mixes in L9 orthogonal arrays. The presence of higher proportions of voids and micro-cracks visible in the SEM images of T1 and T8 mix, which also corresponds to lower compressive strength development. This is because of lower activator dosage resulting into the development of weaker polymerisation, resulting in lower compressive strengths. Continuous gel with fewer micro-pore spaces are visible in micrographs of T2, T3,

Table 8 Optimum mix based on Taguchi and Taguchi GRA methods

Taguchi method		GRA method
Flowability (%)	F-12.5% S-12.5% A-14% W-26%	F-12.5% S-25% A-14% W- 23%
Initial setting time (min)	F-12.5% S-0% A-12% W-26%	
Final setting time (min)	F-25% S-0% A-10% W-26%	
CS 7 days (MPa)	F-12.5% S-25% A-14% W-23%	
CS 28 days (MPa)	F-12.5% S-25% A-14% W-23%	

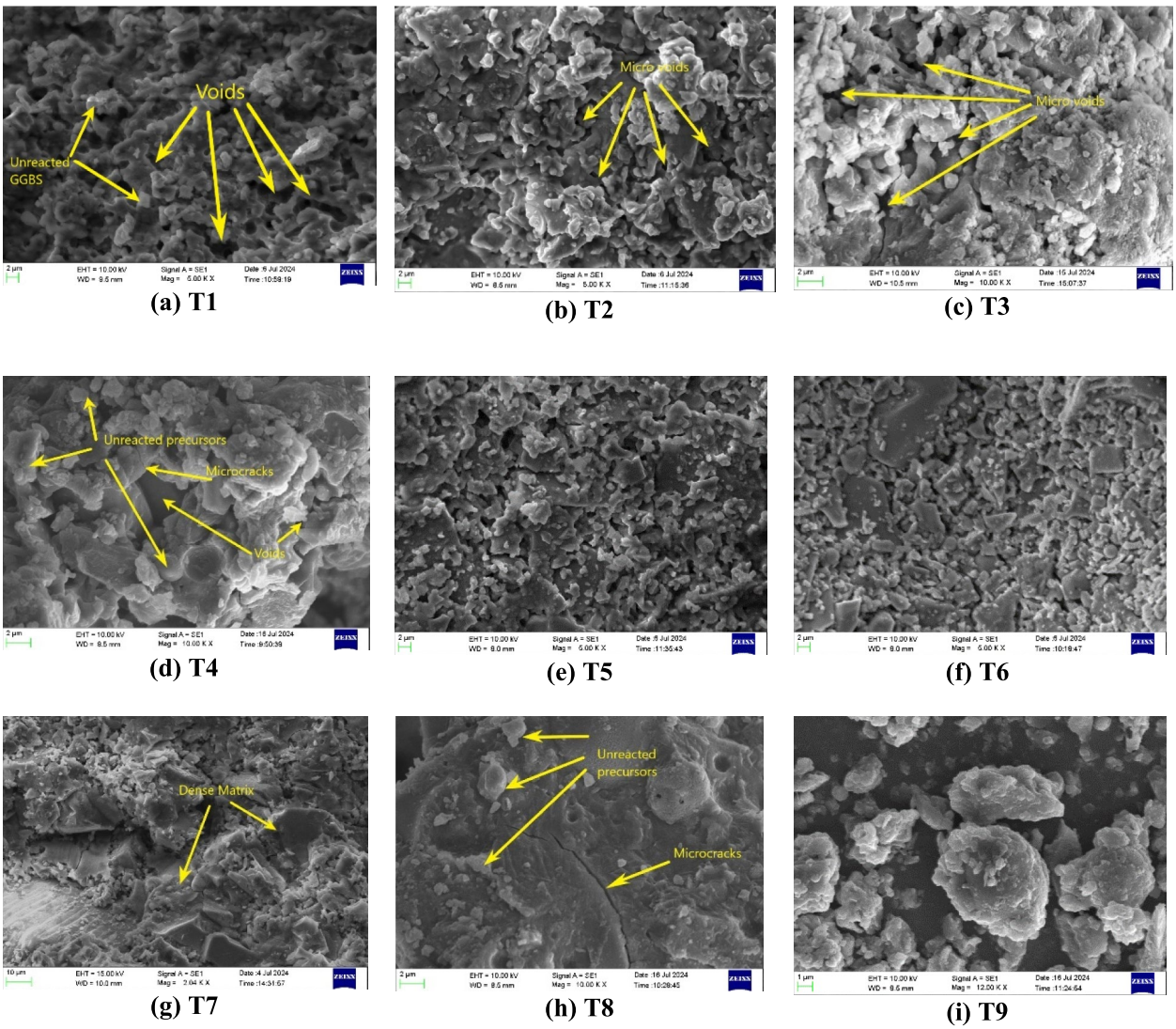

Fig. 10 SEM micrograph of L9 orthogonal binder mixes

Table 10 EDS analysis of L9 array orthogonal mixes

Mix ID	Si	Al	Ca	Na	Si + Al	Si/Al	Ca/(Si + Al)	Na/(Si + Al)	Ca/Si	Na/Al	Na/Si	Ca/Al	Al/Si	*CS (MPa)
T1	43.7	7.32	41.1	7.9	51.01	5.97	0.81	0.15	0.94	1.07	0.18	5.62	0.17	32.00
T2	48.6	12.3	35.1	4	60.9	3.95	0.58	0.07	0.72	0.32	0.08	2.86	0.25	49.45
T3	47.2	9.99	33	9.9	57.18	4.72	0.58	0.17	0.70	0.99	0.21	3.30	0.21	56.11
T4	42.3	17.2	35.9	4.7	59.49	2.46	0.60	0.08	0.85	0.27	0.11	2.09	0.41	47.59
T5	46.1	11.5	32.7	9.8	57.53	4.01	0.57	0.17	0.71	0.85	0.21	2.85	0.25	65.36
T6	58.2	10.8	25.2	5.8	68.98	5.42	0.37	0.08	0.43	0.54	0.10	2.35	0.18	60.74
T7	35.2	19.1	36.5	9.2	54.33	1.84	0.67	0.17	1.04	0.48	0.26	1.91	0.54	64.80
T8	56.5	12.1	25.3	6.2	68.5	4.68	0.37	0.09	0.45	0.51	0.11	2.10	0.21	34.28
T9	61.3	12.1	18.7	7.8	73.44	5.05	0.25	0.11	0.31	0.65	0.13	1.54	0.20	60.00

* CS—compressive strength of binder at 28 days age in MPa

T4 and T9 and T9, hence these mixes are characterised by moderate strength development. These results are further validated through EDS, XRD and FTIR techniques.

The elemental compositions of 28 days ambient cured binder mixes were analysed through EDS analyses. Table 10 shows the EDS analysis results of L9 orthogonal mixes. The presence of Ca, Si, Al, and Na elements are identified. Ca/Si ratios of the mixes ranged between 0.31 and 1.04. Amongst these, the mixes T9 and T6, with Ca/Si ratios of 0.31 and 0.43, respectively, represent the silicate-dominated systems with relatively lower proportions of calcium compounds. This is evident from L9 orthogonal mix compositions, where microsilica is present at a higher level with respect to calcium-rich GGBS. In contrast, T8, which developed relatively lower compressive strength, is characterised with lower proportion of activators and microsilica, exhibits a Ca/Si ratio of 0.45 and Na/Si ratio of 0.11. This could be due to the lower proportion activators that are necessary for the complete initiation of the dissolution and dispersion of precursors, as evident with SEM micrographs of T8. The mixes with higher Ca/Si ratios, specifically 1.04, 0.71, and 0.70 for T7, T5, and T3, respectively, combined with Na/Si ratios of 0.26, 0.21, and 0.21, signify the development of hybrid systems where C-S-H gels coexist with aluminosilicate dense gels, contributing to early setting and subsequent strength development, which is also evident from the setting time and 28-day compressive results of L9 orthogonal arrays results as well as the dense system visible from SEM micrographs (Cheah et al., 2017; Deir et al., 2014; Ma et al., 2018; Yousefi Oderji et al., 2019). However, mixes T1, T4, and T2, despite having higher Ca/Si ratios of 0.94, 0.85, and 0.72, respectively, along with low Na/Si ratios of 0.18, 0.11, and 0.08, respectively, resulted in lower strength development due to the use of lower amount of alkali activators. Figure 11 also shows the comparison of Ca/Si, Ca/(Si + Al), Na/Si, Na/(Si + Al) ratios, with the development of compressive strength. The ratios of Ca/Si and Ca/(Si + Al) display a similar pattern, which is also observed in the ratios of Na/Si and Na/(Si + Al).

The Al/Si ratios of the L9 orthogonal mixes, range from 0.17 to 0.54. The lower Al/Si signifies the development of higher proportions of silica-dominated gel structure and slower setting time, with the limited contribution of alumina to gel structures. However, higher ratios of Al/Si represent contribution in the formation of aluminosilicate gels (NASH) and faster setting times.

3.3.2 FTIR Analysis

FTIR spectra were analysed for the L9 orthogonal array mixes to investigate the reactivity of Ca, Si and Al compounds, in the presence of sodium metasilicate as an activator within the binder matrix. FTIR spectra of all the mixes are presented in Fig. 12. Peak identified at FTIR bands at approximately 535 cm^{-1} and 785 cm^{-1} wavelengths is associated with Si–O–Si, Ca–O–Si and Si–O–Al vibrations, which are often associated with silicates and aluminosilicate structures (Onutai et al., 2023). This indicates the formation of C-A-S-H gel phases as a result of the reaction between sodium metasilicate and calcium oxide, principally present in GGBS, explicitly visible in the T3, T4 and T8 binder matrices. The relative strengths of these mixes are lower than other mixes of

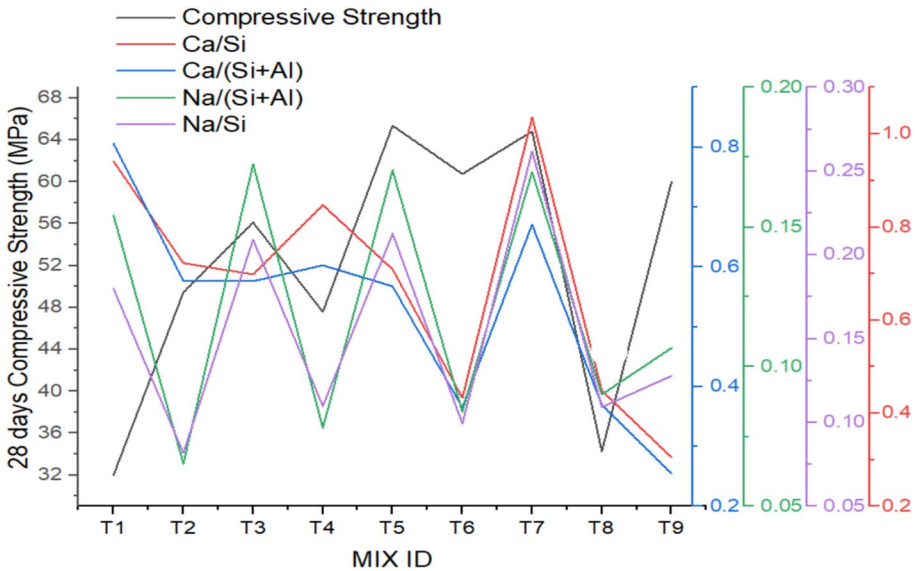

Fig. 11 EDS results of L9 orthogonal binder mixes

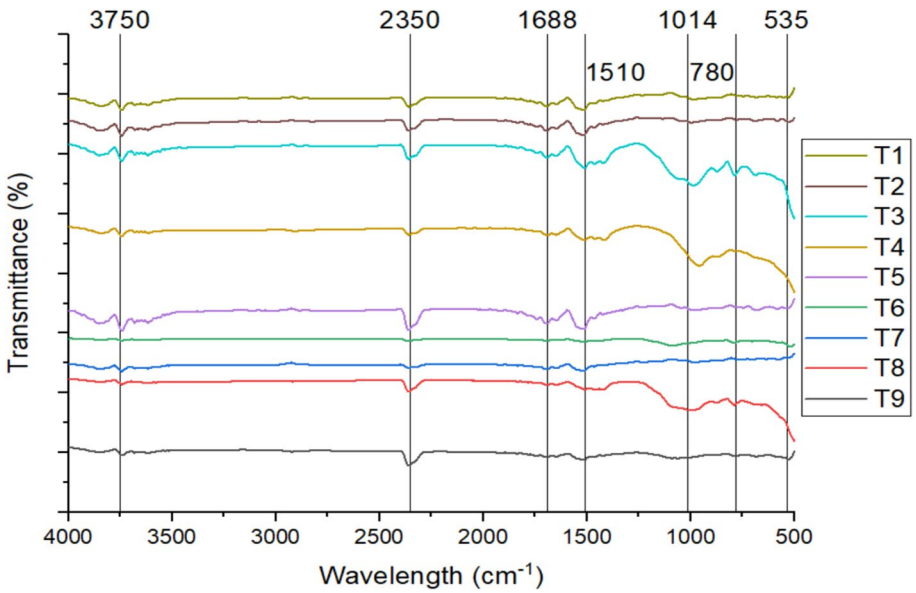

Fig. 12 FTIR spectra for L9 orthogonal mixes

L9 orthogonal arrays, indicating the formation of amorphous or partially crystalline phase of silicate during polymerisation, which are also evident from XRD results. Peak identified in the range of 1014 cm^{-1} is related to Si–O silicate stretching vibration, which in turn may indicate the presence of unreacted or partially reacted aluminosilicates that are present in the precursors. The broader peak of T8, indicates the observed amorphous phase. Sharp shifts in around 1014 cm^{-1} peaks in T3 and T4 may indicate varying degree of polymerisations and interaction of Al, Ca and Na elements identified in the precursors. Peak around 1688 cm^{-1} wavelength, observed in almost all the L9 orthogonal mixes, indicates the presence of hydrated gel phases, resembling H–O–H bending, due to adsorbed water present in C-A-S-H gel. The carboxylate group often produces asymmetric stretching bands around 1500–1600 cm^{-1}. The peaks in this range may be related to formation of calcite.

Peaks identified in the wavelength of 2350 cm^{-1}, corresponding to the asymmetric stretching vibration of carbon dioxide gas, may resembles the similar peaks that were identified in the precursors. Peaks visible at the range of 3750 cm^{-1} are associated with O–H stretching bond of hydroxyl groups. These peaks, that are observed in all the mixes, representing free hydroxyls on the surface, indicating weakly adsorbed moisture that has contributed to this band.

3.3.3 XRD Analysis

XRD analysis provides insights into the crystalline and amorphous phases developed within binder phase system. Figure 13 shows XRD results of all the mixes suggested by L9 orthogonal array observed after 28 days of ambient cured specimens. XRD was observed over a 2θ range from 10^0 to 80^0. The hardened binder specimens, identified peaks pertaining to the crystalline phases such as quartz, calcite, hematite, and mullite, which are also identified in the precursors used in the binders, however, there is variation in their respective intensities. Thus, it can be inferred that the precursors have undergone alkali activation to produce the activation C/N-A-S-H products.

The XRD spectra pertaining to T1, which has lower activator content with 100% GGBS, depict the formation of amorphous gel phases, since no predominant crystalline peaks. On comparing the XRD patterns of T4 and T7, which consists of blends of GGBS and fly-ash, having a relatively higher percentage of activator, exhibit a broad hump between 20^0 and 40^0. This relates to formations of C-S-H and aluminosilicate structures (C-A-S-H) (Ma et al., 2018; Shah et al., 2020). All other mixes exhibit varying intensities of crystalline peaks at approximately 27^0, indicating the presence of non-reactive silica in the form of quartz, which has also been identified in the XRD as shown in Fig. 13. C-(N)-A-S-H gel peaks were observed within the 2θ range of 20° to 40°, signifying the strength development of the binder paste (Kim et al., 2013). The mixes T3, T5, T6, T7 and T9, which have undergone aluminosilicates nucleation, transform into quasi-nanocrystals of zeolitic phase between approximately 20^0 to 70^0 range, are responsible for the strength development. It is also evident from

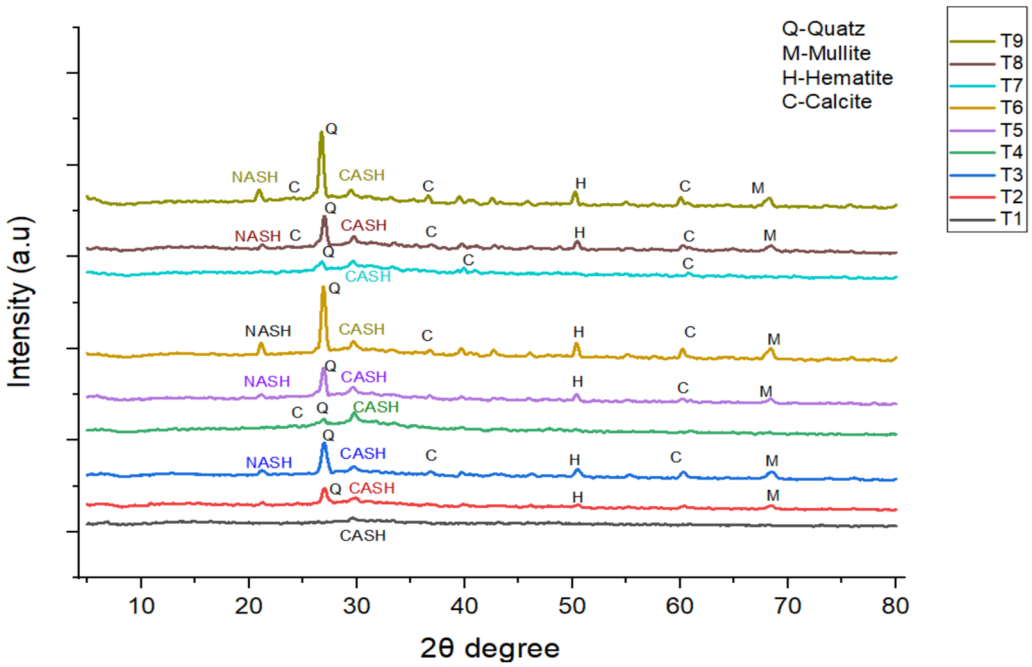

Fig. 13 XRD results of L9 orthogonal mixes

EDS results of mixes T3, T5, T6, T7 and T9 that the higher Ca/Si ratios indicates the formation of hybrid systems where C-S-H gels coexist with aluminosilicate gels, contributing to early-age strength development. This is because GGBS exhibits hydraulic as well as pozzolanic behaviour and all the mixes are dominated by the presence of GGBS as the major precursor.

3.4 Sustainability Assessment: Carbon Emissions and Cost Analysis

The environmental impact of the proposed binder mixes were assessed based on carbon emissions, eco-efficiency, and the cost associated with the materials and processes. These parameters are compared with that of the conventional OPC-based binders. Figure 14 presents the binder

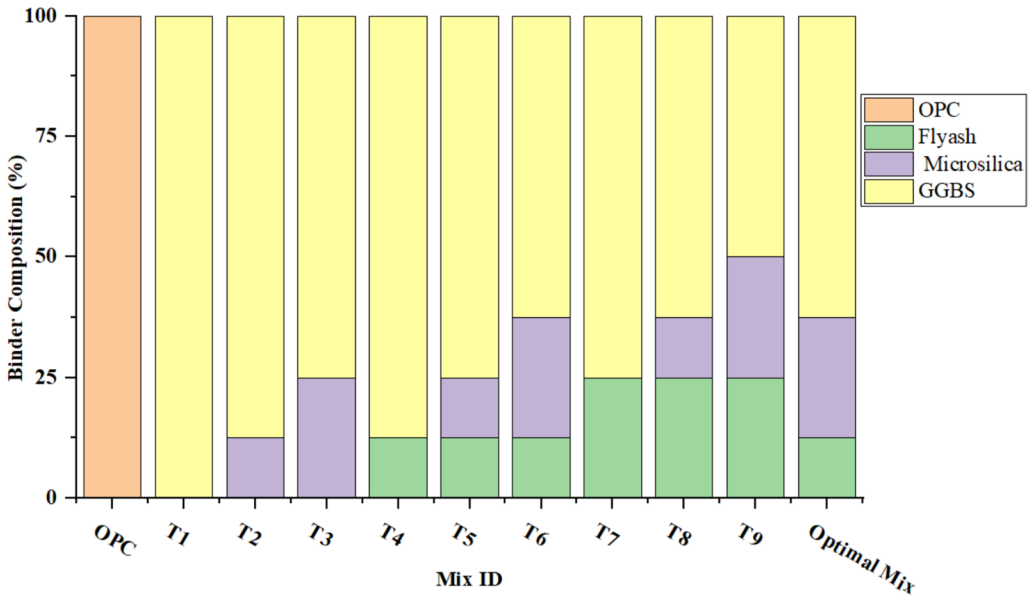

Fig. 14 Percentage of binders used in mixes

composition for the L9 orthogonal mixes along with the proposed optimal mix and the conventional OPC binder. The present study evaluates the carbon emissions, eco-efficiency and cost implications of the mixes for 100 g of cementitious materials and compares them with the OPC-based binder system. The carbon emission and energy consumption factors depend on the availability of raw materials, manufacturing process and the mode of transportation along with the distance to which the materials need to be transported. Hence, representative factors from the literature (Alsalman et al., 2021; Kumar & Prashant, 2024; Kumar et al., 2022; Qiu et al., 2022; Turner & Collins, 2013; Witzleben, 2022) are used, and values are listed in Table 11.

In Fig. 15, the OPC mix exhibits a significantly higher carbon footprint, with a carbon emission of 95.13 (g CO_2-eq/g). Moreover, it also exhibits a relatively higher environmental impact during the cradle-to-gate phase (paper). In contrast, all other mixes demonstrate a substantial reduction in carbon emissions. The lowest emissions were observed for T1 (8.52 g CO_2-eq/g), followed by T4 (9.9 g CO_2-eq/g) and T7 (11.27 g CO_2-eq/g), indicating their excellent environmental performance. Even the mixes with relatively higher emissions, such as T3 (22.4 g CO_2-eq/g), T9 (20.76 g CO_2-eq/g), and the Optimal Mix (22.31 g CO_2-eq/g), still achieve over a 70% reduction compared to OPC.

The optimal mix, despite being tailored for balanced mechanical and fresh-state properties, maintains a considerably reduced carbon footprint. This highlights the feasibility of achieving both performance and sustainability targets in AAB systems. The slight variation in emissions across mixes can be attributed to the type and dosage of precursors and alkaline activators used, particularly materials like sodium metasilicate, which have higher embedded emissions. Overall, the results confirm that alkali-activated binders offer a promising low-carbon alternative to OPC.

The eco-efficiency is evaluated in terms of the ratio of compressive strength to carbon dioxide emissions, providing a measure of sustainability performance assessment. The results are compared against OPC at both 7 and 28 days, as illustrated in Fig. 16. OPC binder exhibits the lowest eco-efficiency, with values of 0.36 MPa/g CO_2-eq/g and 0.59 MPa/g CO_2-eq/g at 7 and 28 days,

Table 11 Carbon emission values

Raw materials	Total emission (kg CO_2-eq/kg)
Cement|	0.951
Flyash	0.005
Microsilica	0.45
GGBS	0.012
Sodium metasilicate	0.73
Water	0.1

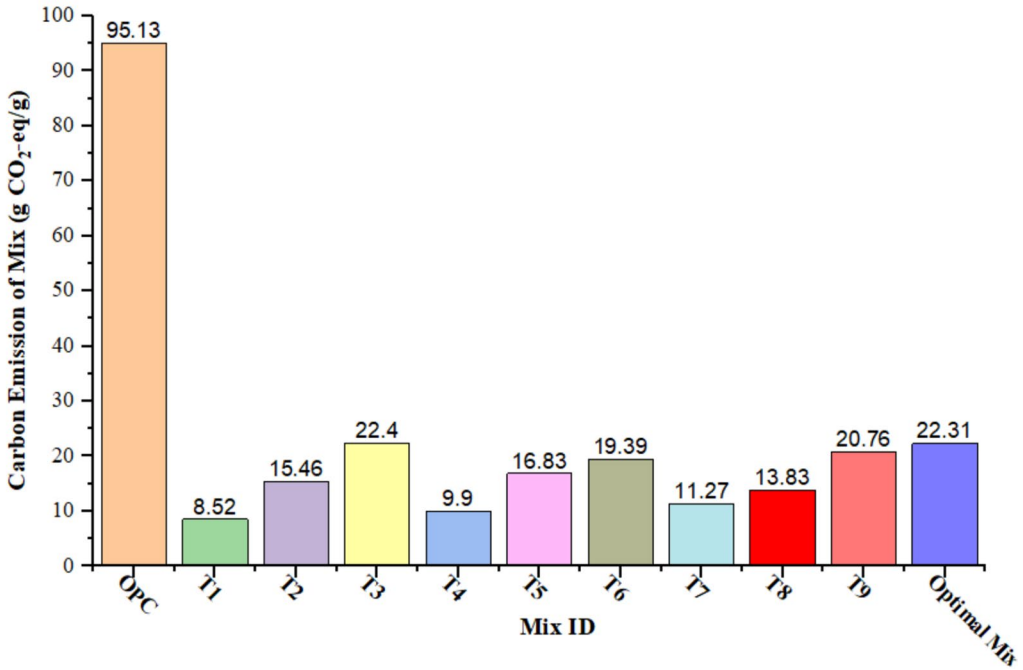

Fig. 15 Total carbon emissions of proposed mixes

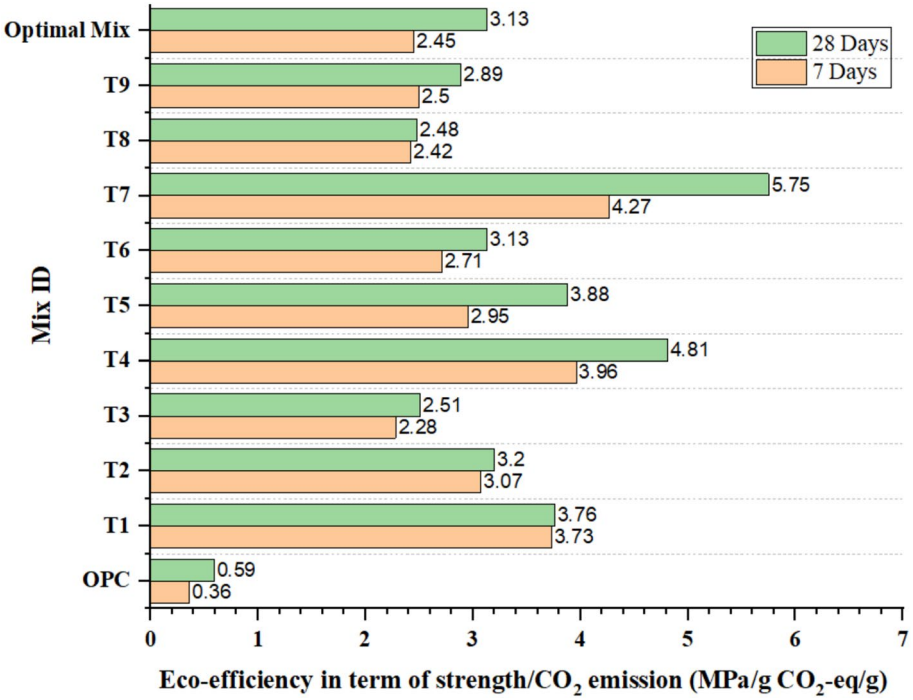

Fig. 16 Eco-efficiency compressive strength/CO2 emissions (MPa/g CO_2-eq/g)

respectively. This indicates its high carbon intensity relative to the strength achieved. In contrast, all other mixes of AAB demonstrate significantly higher eco-efficiency values, validating their potential as sustainable alternatives. Amongst the AABs presented in the L9 orthogonal matrix, the mix T7 exhibits the highest eco-efficiency, reaching 5.75 MPa/g CO_2-eq/g at 28 days and 4.27 MPa/g CO_2-eq/g at 7 days, reflecting its balance of strength gain and low emissions. Mix T4 and Mix T5 also perform remarkably well, with eco-efficiency values of 4.81 MPa/g CO_2-eq/g and 3.88 MPa/g CO_2-eq/g at 28 days, respectively. Even optimal mixes with eco-efficiency of 3.13 MPa/g CO_2-eq/g at 28 days, outperform OPC, which were primarily designed for balanced fresh and hardened properties. The increase in eco-efficiency from 7 to 28 days in all mixes indicates that AABs gain strength more efficiently over time with a minimal increase in emissions. This further enhances their sustainability factors for structural applications.

The cost of the conventional OPC mix is 9 rupees per 100 g, which is comparably lower than the proposed mixes as illustrated in Fig. 17. However, despite its low cost, OPC delivers a compressive strength of 55 MPa, which is comparable to AAB mixes. Amongst the AAB binder systems, T3 exhibits the highest cost of 15.55 rupees, followed closely by the Optimal Mix at 15.425 rupees and T9 cost at 14.4 rupees. These mixes deliver relatively higher strength, however, they are associated with higher cost due to the higher usage of activators or microsilica. However, these mixes exhibit excellent mechanical strength along with strong eco-efficiency and a lower carbon footprint. Although OPC remains economical, AAB mixes performing better in terms of eco-efficiency, mechanical strength and carbon footprint. By using activators derived from by-products, the cost may be reduced without compromising its mechanical performance and sustainability aspects.

4 Conclusion

- A one-part alkali-activated binder is not only a viable solution for in situ applications, but also a necessity to futuristic sustainable alternative construction materials for large-scale applications. By carefully adjusting the proportions of precursors and activator, the fresh and hardened properties of ternary blended AAB can be tailored and optimised to meet required performance criteria.
- AAB properties are governed by distinct yet interdependent factors: flowability by water content, setting times by activator dosage, and strength by precursors. Taguchi's GRA optimisation effectively balances these parameters for optimal performance. Experimental validation confirms the reliability of Taguchi results, exhibiting an error margin within 6%.

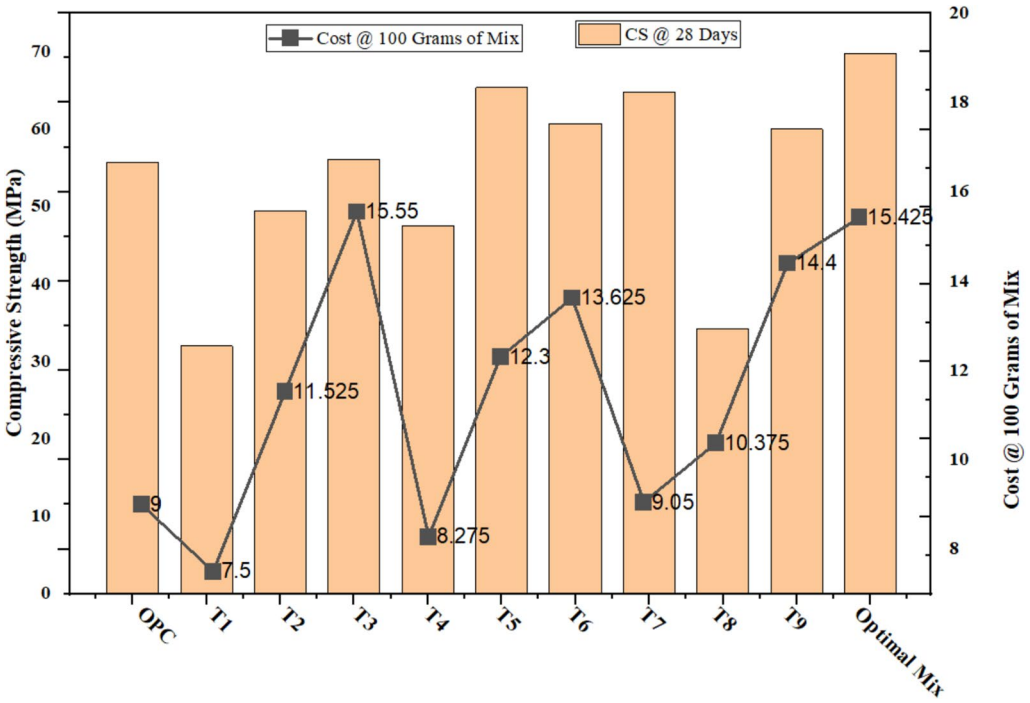

Fig. 17 Cost analysis of L9 orthogonal mixes (in Rupees)

- Optimised slag–flyash–microsilica ternary one-part AAB system developed using Taguchi-GRA methodology presents the fresh properties (120% flowability, 46–95 min setting times) and high compressive strengths (54.65–69.75 MPa), suitable for high strength commercial applications, while being more sustainable and user-friendly. Microstructural analyses confirmed the presence of a dense matrix of C/N-A-S-H and CSH gels within the ternary blended alkali-activated system.
- The optimised ternary blended AAB mix reduced CO_2 emissions by 75% compared to OPC while achieving a high compressive strength of 69.75 MPa. Though the mix is slightly costlier, it offers superior eco-efficiency, proving AABs can balance performance and sustainability.

5 Future Scope

A detailed study on early-age reaction kinetics of the one-part ternary system using microanalytical techniques to explain phase evolution under ambient conditions will enable in setting standards for precursor dosage and activator combinations for various levels of performance. The role of microsilica in enhancing gel formation through nucleation effects needs further investigation. Exploring hybrid activators could offer a balance between performance and cost. Additionally, long-term durability assessment of the optimal mix is essential to understand its performance.

Abbreviations

GRA	Taguchi grey relational analysis
IST	Initial setting time
FST	Final setting time
SEM	Scanning electron microscope
EDS	Energy dispersive X-ray spectroscopy
XRD	X-ray diffraction
FTIR	Fourier transform infrared spectroscopy
C-A-S–H	Calcium alumino silicate hydrate
N-A-S–H	Sodium alumino silicate hydrate
OPC	Ordinary portland cement
AAB	Alkali activated binder
AAM	Alkali activated material
AAC	Alkali activated concrete
GGBS	Ground granulated blast furnace slag
C-S–H	Calcium silicate hydrate
DOE	Design of experiment
ANOVA	Analysis of variance
DF	Degrees of freedom
SS	Sum of squares
MS	Mean square
CS	Compressive strength

Acknowledgements

The authors thank the department for providing the facilities necessary to carry out the experiments presented in the manuscript.

Author contributions

The study was designed with contributions from all authors. H M Jagadisha: conceptualisation, methodology, validation, formal analysis, investigation, writing—original draft, visualisation. Poornachandra Pandit: conceptualisation, methodology, writing—review and editing, supervision. Shreelaxmi Prashant: conceptualisation, methodology, writing—review and editing, supervision. Lalit Bhole: methodology, data collection. Yashodhan Singh: methodology,

data collection. Ojas Verma: methodology, data collection. Mithesh Kumar: methodology, data collection, writing—review and editing. Finally, all authors reviewed and approved the final document.

Funding
Open access funding provided by Manipal Academy of Higher Education, Manipal. The authors have no relevant financial or non-financial interests to disclose.

Data availability
All data generated or analysed during this study are included in this published article.

Declarations

Ethics approval and consent to participate
Not applicable.

Consent for publication
All authors of the manuscript agree on the publication of this work in the *International Journal of Concrete Structures and Materials*.

Competing interests
No competing interests exits in the submission of this manuscript, and manuscript is approved by all authors for publication. The author declare that the work described was original research that has not been published previously, and not under consideration for publication elsewhere, in whole or in part.

Author details
[1]Department of Civil Engineering, Manipal Institute of Technology, Manipal Academy of Higher Education, Manipal 576104, India.

Received: 22 March 2025 Accepted: 1 July 2025
Published online: 29 August 2025

References

Alhassan, M., Alkhawaldeh, A., Betoush, N., Alkhawaldeh, M., Huseien, G. F., Amaireh, L., & Elrefae, A. (2023). Life cycle assessment of the sustainability of alkali-activated binders. *Biomimetics, 8*(1), 58. https://doi.org/10.3390/biomimetics8010058

Alsalman, A., Assi, L. N., Kareem, R. S., Carter, K., & Ziehl, P. (2021). Energy and CO2 emission assessments of alkali-activated concrete and Ordinary Portland Cement concrete: A comparative analysis of different grades of concrete. *Cleaner Environmental Systems, 3*, 100047. https://doi.org/10.1016/J.CESYS.2021.100047

Amer, I., Abdelkhalik, A., Mayhoub, O. A., & Kohail, M. (2024). Development of Sustainable slag-based geopolymer concrete using different types of chemical admixtures. *International Journal of Concrete Structures and Materials*. https://doi.org/10.1186/s40069-024-00672-1

Amer, I., Kohail, M., El-Feky, M. S., Rashad, A., & Khalaf, M. A. (2021). Characterization of alkali-activated hybrid slag/cement concrete. *Ain Shams Engineering Journal, 12*(1), 135–144. https://doi.org/10.1016/j.asej.2020.08.003

ASTM C1437-01: Standard Test Method for Flow of Hydraulic Cement Mortar. (2020). ASTM.

Cheah, C. B., Samsudin, M. H., Ramli, M., Part, W. K., & Tan, L. E. (2017). The use of high calcium wood ash in the preparation of Ground Granulated Blast Furnace Slag and Pulverized Fly Ash geopolymers: A complete microstructural and mechanical characterization. *Journal of Cleaner Production, 156*, 114–123. https://doi.org/10.1016/J.JCLEPRO.2017.04.026

Deir, E., Gebregziabiher, B. S., & Peethamparan, S. (2014). Influence of starting material on the early age hydration kinetics, microstructure and composition of binding gel in alkali activated binder systems. *Cement and Concrete Composites, 48*, 108–117. https://doi.org/10.1016/J.CEMCONCOMP.2013.11.010

Ding, Y., Dai, J. G., & Shi, C. J. (2016). Mechanical properties of alkali-activated concrete: A state-of-the-art review. *Construction and Building Materials, 127*, 68–79. https://doi.org/10.1016/j.conbuildmat.2016.09.121

Elahi, M. M. A., Hossain, M. M., Karim, M. R., Zain, M. F. M., & Shearer, C. (2020). A review on alkali-activated binders: Materials composition and fresh properties of concrete. *Construction and Building Materials, 260*, 119788. https://doi.org/10.1016/J.CONBUILDMAT.2020.119788

Faridmehr, I., Fahim Huseien, G., & Hajmohammadian Baghban, M. (2020). Evaluation of mechanical and environmental properties of engineered alkali-activated green mortar. *Materials, 13*(18), 4098. https://doi.org/10.3390/ma13184098

Farooq, F., Jin, X., Faisal Javed, M., Akbar, A., Izhar Shah, M., Aslam, F., & Alyousef, R. (2021). Geopolymer concrete as sustainable material: A state of the art review. *Construction and Building Materials, 306*, 124762. https://doi.org/10.1016/j.conbuildmat.2021.124762

Fernández-Jiménez, A., Palomo, A., & Criado, M. (2005). Microstructure development of alkali-activated fly ash cement: A descriptive model. *Cement and Concrete Research, 35*(6), 1204–1209. https://doi.org/10.1016/j.cemconres.2004.08.021

Geraldo, R. H., Gonçalves, J. P., & Camarini, G. (2023). Mechanical properties of an eco-friendly one-part alkali-activated binder: Influence of metakaolin and water content. *Ceramics International, 49*(8), 11854–11864. https://doi.org/10.1016/J.CERAMINT.2022.12.032

Gok, S. G., & Sengul, O. (2024). Enhancing mechanical properties of alkali-activated slag SIFCON for sustainable construction using recycled glass and tire-derived waste steel fibers. *International Journal of Concrete Structures and Materials*. https://doi.org/10.1186/s40069-024-00724-6

Hadi, M. N. S., Farhan, N. A., & Sheikh, M. N. (2017). Design of geopolymer concrete with GGBFS at ambient curing condition using Taguchi method. *Construction and Building Materials, 140*, 424–431. https://doi.org/10.1016/j.conbuildmat.2017.02.131

Hamada, H. M., Abed, F., Binti Katman, H. Y., Humada, A. M., Al Jawahery, M. S., Majdi, A., Yousif, S. T., & Thomas, B. S. (2023). Effect of silica fume on the properties of sustainable cement concrete. *Journal of Materials Research and Technology, 24*, 8887–8908. https://doi.org/10.1016/J.JMRT.2023.05.147

Hamsashree, Pandit, P., Prashanth, S., & Katpady, D. N. (2024). Durability of alkali-activated fly ash-slag concrete- state of art. *Innovative Infrastructure Solutions*. https://doi.org/10.1007/s41062-024-01530-5

IS 12269: Ordinary Portland Cement, 53 Grade—Specification. (2013). Bureau of Indian Standards. https://bis.gov.in/

IS 4031-5: Methods of physical tests for hydraulic cement, Part 5: Determination of initial and final setting times. (2005). Bureau of Indian Standards. https://bis.gov.in/

IS 4031-6: Methods of Physical Tests for Hydraulic Cement Part 6: Determination of compressive strength of hydraulic cement other than masonry cement. (2005). Bureau of Indian Standards. https://bis.gov.in/

IS 5512: Specification for flow table for use in tests of hydraulic cements and pozzolanic materials. (1983). Bureau of Indian Standards. https://bis.gov.in

Jaradat, Y., & Matalkah, F. (2023). Effects of micro silica on the compressive strength and absorption characteristics of olive biomass ash-based geopolymer. *Case Studies in Construction Materials, 18*, Article e01870. https://doi.org/10.1016/J.CSCM.2023.E01870

Jeffrey Kuo, C.-F., Su, T.-L., Jhang, P.-R., Huang, C.-Y., & Chiu, C.-H. (2011). Using the Taguchi method and grey relational analysis to optimize the flat-plate collector process with multiple quality characteristics in solar energy collector manufacturing. *Energy, 36*(5), 3554–3562. https://doi.org/10.1016/j.energy.2011.03.065

Kamath, M., Prashant, S., & Kumar, M. (2021). Micro-characterisation of alkali activated paste with fly ash-GGBS-metakaolin binder system with ambient setting characteristics. *Construction and Building Materials, 277*, 122323. https://doi.org/10.1016/J.CONBUILDMAT.2021.122323

Kanagaraj, B., Anand, N., Alengaram, U. J., Raj, R. S., Praveen, B., & Tattukolla, K. (2022). Performance evaluation on engineering properties and sustainability analysis of high strength geopolymer concrete. *Journal of Building Engineering*. https://doi.org/10.1016/j.jobe.2022.105147

Karthik, S., & Mohan, K. S. R. (2021). A Taguchi approach for optimizing design mixture of geopolymer concrete incorporating fly ash, ground granulated blast furnace slag and silica fume. *Crystals*. https://doi.org/10.3390/cryst11111279

Kim, M. S., Jun, Y., Lee, C., & Oh, J. E. (2013). Use of CaO as an activator for producing a price-competitive non-cement structural binder using ground granulated blast furnace slag. *Cement and Concrete Research, 54*, 208–214. https://doi.org/10.1016/J.CEMCONRES.2013.09.011

Kumar, M., & Prashant, S. (2024). Durability and ecological evaluation of structural concrete with sewage sludge ash as ternary binder. *Civil Engineering and Architecture, 12*(2), 1143–1164. https://doi.org/10.13189/cea.2024.120234

Kumar, M., Prashant, S., & Kamath, M. V. (2022). Enhancing the sustainability of high strength concrete in terms of embodied energy and carbon emission by incorporating sewage sludge and fly ash. *Innovative Infrastructure Solutions, 7*(4), 240. https://doi.org/10.1007/s41062-022-00837-5

Luukkonen, T., Abdollahnejad, Z., Yliniemi, J., Kinnunen, P., & Illikainen, M. (2018). One-part alkali-activated materials: A review. *Cement and Concrete Research, 103*, 21–34. https://doi.org/10.1016/J.CEMCONRES.2017.10.001

Ma, C., Long, G., Shi, Y., & Xie, Y. (2018). Preparation of cleaner one-part geopolymer by investigating different types of commercial sodium metasilicate in China. *Journal of Cleaner Production, 201*, 636–647. https://doi.org/10.1016/J.JCLEPRO.2018.08.060

Mahendra, K., Narasimhan, M. C., Prakash, G. B., & Das, A. K. (2024). Experimental investigation and optimization of one-part alkali-activated self-compacting concrete mixes. *Case Studies in Construction Materials, 21*, Article e04062. https://doi.org/10.1016/J.CSCM.2024.E04062

Martinez-Lopez, R., & Ivan Escalante-Garcia, J. (2016). Alkali activated composite binders of waste silica soda lime glass and blast furnace slag: Strength as a function of the composition. *Construction and Building Materials, 119*, 119–129. https://doi.org/10.1016/j.conbuildmat.2016.05.064

Metkar, R. M., Sunnapwar, V. K., Hiwase, S. D., Anki, V. S., & Dumpa, M. (2013). Evaluation of FEM based fracture mechanics technique to estimate life of an automotive forged steel crankshaft of a single cylinder diesel engine. *Procedia Engineering, 51*, 567–572. https://doi.org/10.1016/j.proeng.2013.01.080

Mustakim, S. M., Das, S. K., Mishra, J., Aftab, A., Alomayri, T. S., Assaedi, H. S., & Kaze, C. R. (2021). Improvement in fresh, mechanical and microstructural properties of fly ash- Blast furnace slag based geopolymer concrete by addition of nano and micro silica. *SILICON, 13*(8), 2415–2428. https://doi.org/10.1007/S12633-020-00593-0

Mustapha, A. N., Zhang, Y., Zhang, Z., Ding, Y., Yuan, Q., & Li, Y. (2021). Taguchi and ANOVA analysis for the optimization of the microencapsulation of a volatile phase change material. *Journal of Materials Research and Technology, 11*, 667–680. https://doi.org/10.1016/J.JMRT.2021.01.025

Najm, O., El-Hassan, H., & El-Dieb, A. (2022). Optimization of alkali-activated ladle slag composites mix design using Taguchi-based TOPSIS method. *Construction and Building Materials, 327*, 126946. https://doi.org/10.1016/J.CONBUILDMAT.2022.126946

Onutai, S., Osugi, T., & Sone, T. (2023). Alumino-silicate structural formation during alkali-activation of metakaolin: In-Situ and Ex-Situ ATR-FTIR studies. *Materials, 16*(3), 985. https://doi.org/10.3390/ma16030985

Panagiotopoulou, C., Tsivilis, S., & Kakali, G. (2015). Application of the Taguchi approach for the composition optimization of alkali activated fly ash binders. *Construction and Building Materials, 91*, 17–22. https://doi.org/10.1016/J.CONBUILDMAT.2015.05.005

Perumal, P., Sreenivasan, H., Luukkonen, T., Kantola, A. M., Telkki, V.-V., Kinnunen, P., & Illikainen, M. (2021). High strength one-part alkali-activated slag blends designed by particle packing optimization. *Construction and Building Materials, 299*, 124004. https://doi.org/10.1016/j.conbuildmat.2021.124004

Provis, J. L., & Bernal, S. A. (2014). Geopolymers and related alkali-activated materials. *Annual Review of Materials Research, 44*(1), 299–327. https://doi.org/10.1146/annurev-matsci-070813-113515

Puligilla, S., & Mondal, P. (2013). Role of slag in microstructural development and hardening of fly ash-slag geopolymer. *Cement and Concrete Research, 43*(1), 70–80. https://doi.org/10.1016/J.CEMCONRES.2012.10.004

Qiu, Y., Pan, H., Zhao, Q., Zhang, J., Zhang, Y., & Guo, W. (2022). Carbon dioxide-hardened sodium silicate-bonded sand regeneration using calcium carbide slag: The design and feasibility study. *Journal of Environmental Chemical Engineering, 10*(3), 107872. https://doi.org/10.1016/J.JECE.2022.107872

Rawat, S., Zhang, Y. X., & Lee, C. K. (2022). Multi-response optimization of hybrid fibre engineered cementitious composite using Grey-Taguchi method and utility concept. *Construction and Building Materials, 319*, 126040. https://doi.org/10.1016/j.conbuildmat.2021.126040

Rossi, L., de Lima, L. M., Sun, Y., Dehn, F., Provis, J. L., Ye, G., & De Schutter, G. (2022). Future perspectives for alkali-activated materials: from existing standards to structural applications. *RILEM Technical Letters, 7*, 159–177. https://doi.org/10.21809/rilemtechlett.2022.160

Rostami, M., & Behfarnia, K. (2017). The effect of silica fume on durability of alkali activated slag concrete. *Construction and Building Materials, 134*, 262–268. https://doi.org/10.1016/J.CONBUILDMAT.2016.12.072

Segura, I. P., Luukkonen, T., Yliniemi, J., Sreenivasan, H., Damø, A. J., Jensen, L. S., Canut, M., Kantola, A. M., Telkki, V. V., & Jensen, P. A. (2022). Comparison of One-Part and Two-Part Alkali-Activated Metakaolin and Blast Furnace Slag. *Journal of Sustainable Metallurgy, 8*(4), 1816–1830. https://doi.org/10.1007/s40831-022-00606-9

Shah, S. F. A., Chen, B., Oderji, S. Y., Haque, M. A., & Ahmad, M. R. (2020). Improvement of early strength of fly ash-slag based one-part alkali activated mortar. *Construction and Building Materials, 246*, 118533. https://doi.org/10.1016/J.CONBUILDMAT.2020.118533

Sheelavantar, P. G., Pandit, P., Prashanth, S., Nishit, N., & Jadhav, M. (2024). Taguchi-integrated grey relational analysis for multi-response optimization of mix design for alkali-activated concrete. *Materials Research Express, 11*(7), 075505. https://doi.org/10.1088/2053-1591/ad592c

Shen, D.-H., & Du, J.-C. (2005). Application of gray relational analysis to evaluate HMA with reclaimed building materials. *Journal of Materials in Civil Engineering, 17*(4), 400–406. https://doi.org/10.1061/(ASCE)0899-1561(2005)17:4(400)

Singh, N. B., & Middendorf, B. (2020). Geopolymers as an alternative to Portland cement: An overview. *Construction and Building Materials*. https://doi.org/10.1016/J.CONBUILDMAT.2019.117455

Srinivasa, A. S., Swaminathan, K., & Yaragal, S. C. (2023). Microstructural and optimization studies on novel one-part geopolymer pastes by Box–Behnken response surface design method. *Case Studies in Construction Materials, 18*, Article e01946. https://doi.org/10.1016/j.cscm.2023.e01946

Szabó, R., & Mucsi, G. (2020). Effect of microsilica on the structure and mechanical properties of fly ash-based geopolymer. *Muszaki Foldtudomanyi Kozlemenyek, 89*(2), 68–76.

Thatikonda, N., Mallik, M., Rao, S. V., Madduru, S. R. C., & Dora, T. R. K. (2024). Influential studies on microsilica as a potential replacement for fly ash-GGBFS in self-compacting geopolymer concrete: Microstructural insights and performance analysis. *Journal of Building Pathology and Rehabilitation*. https://doi.org/10.1007/s41024-024-00422-6

Turner, L. K., & Collins, F. G. (2013). Carbon dioxide equivalent (CO2-e) emissions: A comparison between geopolymer and OPC cement concrete. *Construction and Building Materials, 43*, 125–130. https://doi.org/10.1016/j.conbuildmat.2013.01.023

Wang, F., Sun, X., Tao, Z., & Pan, Z. (2022). Effect of silica fume on compressive strength of ultra-high-performance concrete made of calcium aluminate cement/fly ash based geopolymer. *Journal of Building Engineering, 62*, 105398. https://doi.org/10.1016/j.jobe.2022.105398

Witzleben, S. (2022). Minimizing the global warming potential with geopolymer-based insulation material with miscanthus fiber. *Polymers, 14*(15), 3191. https://doi.org/10.3390/polym14153191

Xi, J., Liu, J., Yang, K., Zhang, S., Han, F., Sha, J., & Zheng, X. (2022). Role of silica fume on hydration and strength development of ultra-high performance concrete. *Construction and Building Materials, 338*, 127600. https://doi.org/10.1016/j.conbuildmat.2022.127600

Yousefi Oderji, S., Chen, B., Ahmad, M. R., & Shah, S. F. A. (2019). Fresh and hardened properties of one-part fly ash-based geopolymer binders cured at room temperature: Effect of slag and alkali activators. *Journal of Cleaner Production, 225*, 1–10. https://doi.org/10.1016/J.JCLEPRO.2019.03.290

Yusslee, E., & Beskhyroun, S. (2023). The effect of water-to-binder ratio (W/B) on pore structure of one-part alkali activated mortar. *Heliyon, 9*(1), Article e12983. https://doi.org/10.1016/J.HELIYON.2023.E12983

Publisher's Note

H. M. Jagadisha Assistant Professor, Department of Civil Engineering, Manipal Institute of Technology, Manipal Academy of Higher Education, Manipal-576104, India

Poornachandra Pandit Associate Professor, Department of Civil Engineering, Manipal Institute of Technology, Manipal Academy of Higher Education, Manipal-576104, India.

Shreelaxmi Prashant Associate Professor, Department of Civil Engineering, Manipal Institute of Technology, Manipal Academy of Higher Education, Manipal-576104, India.

Lalit Bhole Under Graduate student, Department of Civil Engineering, Manipal Institute of Technology, Manipal Academy of Higher Education, Manipal-576104, India.

Yashodhan Singh Under Graduate student, Department of Civil Engineering, Manipal Institute of Technology, Manipal Academy of Higher Education, Manipal-576104, India.

Ojas Verma Under Graduate student, Department of Civil Engineering, Manipal Institute of Technology, Manipal Academy of Higher Education, Manipal-576104, India.

Mithesh Kumar PhD Student, Department of Civil Engineering, Manipal Institute of Technology, Manipal Academy of Higher Education, Manipal-576104, India.